JPET Fast Forward. Published on March 19, 2018 as DOI: 10.1124/jpet.117.247163
This article has not been copyedited and formatted. The final version may differ from this version.

Identification and Characterization of Novel Receptor Interacting Serine/threonine-Protein Kinase 2 (RIPK2) Inhibitors Using Structural Similarity Analysis

Mohamed Salla, Rodrigo Aguayo-Ortiz, Danmaliki G. Ibrahim, Alaa Zare, Ahmed Said, Jack Moore, Vrajeshkumar Pandya, Robin Manaloor, Sunny Fong, Anna R. Blankstein, Spencer B. Gibson, Laura Ramos Garcia, Pascal Meier, Khushwant Singh Bhullar, Basil P. Hubbard, Yahya Fiteh, Harissios Vliagoftis, Ing Swie Goping, Dion Brocks, Peter Hwang, Carlos A. Velázquez-Martínez and Shairaz Baksh

Departments of Biochemistry (M.S.; D.G.I.; A.S.; J.K. V.P.; I.N.G.; P.H. S.B.), Pediatrics (A.Z.; R. M.; S.F.; S.B.), Pharmacology (K.S.B.; B.P.H), Oncology (S.B.) Medicine (Y.H.; H.V, P.H) and Faculty of Pharmacy and Pharmaceutical Sciences (R.A.O.; D.B.; C.V.M.) University of Alberta 113 Street 87 Avenue, Edmonton, Alberta, Canada. T6G 2E1. Facultad de Química, Departamento de Farmacia, Universidad Nacional Autónoma de México (R.A.O.) Departments of Biochemistry and Medical Genetics and Immunology (A.R.B.; S.B.G.;) University of Manitoba. Breakthrough Breast Cancer Research Center (L.R.G.; P.M.) Chester Beatty Laboratories 237 Fulham Road, London, UK SW3 6JB. Cancer Research Institute of Northern Alberta (S.B.), Edmonton, AB, Canada. T6G 2R7) and Women and Children's Health Research Institute (S.B.) (4-081 Edmonton Clinic Health Academy [ECHA] 11405 87 Avenue NW Edmonton, AB T6G 1C9)

JPET Fast Forward. Published on March 19, 2018 as DOI: 10.1124/jpet.117.247163
This article has not been copyedited and formatted. The final version may differ from this version.

Running Title: Identification of Novel RIPK2 Inhibitors

Corresponding author:
Shairaz Baksh, Ph. D.
AHFMR Scholar
Associate Professor, Pediatrics
Adjunct Associate Professor, Oncology and Biochemistry
Division of Hematology/Oncology, Department of Pediatrics,
Faculty of Medicine and Dentistry
3-020E Katz Group Centre for Pharmacy and Health Research
113 St. 87 Ave., University of Alberta, Edmonton, AB, Canada.T6G 2E1
Office: 780-492-3494; Lab: 780-492-4000; Fax: 780-492-0723
http://www.bakshlab.com/; http://www.precisionbiomics.com/
RASSF Symposia Information at http://rassfsymposia.com/
Email: sbaksh@ualberta.ca

Number of text pages: 33

Number of tables: 2 (with 2 supplemental tables)

Number of figures: 6 (with 7 supplemental figures)

Number of references: 50

Number of words in the Abstract: 127

Number of words in the Introduction: 678

Number of words in the Discussion: 1344

Non-standard abbreviations: RIPK2, Receptor interacting protein kinase 2; TLR, Toll like receptors; MDP, Muramyl Dipeptide; DSS, Dextran Sulfate Sodium; DAI, Disease activity index; BAL, broncho-alveolar lavage; PAINS, Pan Assay Interference Compounds; ROE, rotating-frame nuclear Overhauser enhancement; MPTP, mitochondrial permeability transition pore; UC, Ulcerative colitis; IBD, Inflammatory Bowel Disease; RASSF1A, *R*as *ass*ociation domain *f*amily protein *1A*; CRC, Colorectal Cancer; PSC, Primary sclerosing cholangitis; NOD2, Nucleotide-binding oligomerization domain-containing protein 2; SIRT1, Sirtuin 1; NFκB, nuclear factor kappa-light-chain-enhancer of activated B cells; PCFP, PubChem Fingerprint; EMT, epithelial to mesenchymal transition; PRRs, pathogen recognition receptors.

JPET Fast Forward. Published on March 19, 2018 as DOI: 10.1124/jpet.117.247163
This article has not been copyedited and formatted. The final version may differ from this version.

Abstract

Receptor interacting protein kinase 2 (RIP2 or RICK herein referred to as RIPK2) is linked to the pathogen pathway that activates NFκB and autophagic activation. Using molecular modeling (docking) and chemoinformatics analyses we utilized the RIPK2/ponatinib crystal structure and searched in chemical databases for small molecules exerting binding interactions similar to those exerted by ponatinib. The identified RIPK2 inhibitors potently inhibited the proliferation of cancer cells by > 70% as well as inhibition of NFκB activity. More importantly, *in vivo* inhibition of intestinal and lung inflammation rodent models suggest effectiveness to resolve inflammation with low toxicity to the animals. Thus, our identified RIPK2 inhibitor may offer a possible therapeutic control of inflammation in diseases such as inflammatory bowel disease, asthma, cystic fibrosis, primary sclerosing cholangitis and pancreatitis.

Visual Abstract

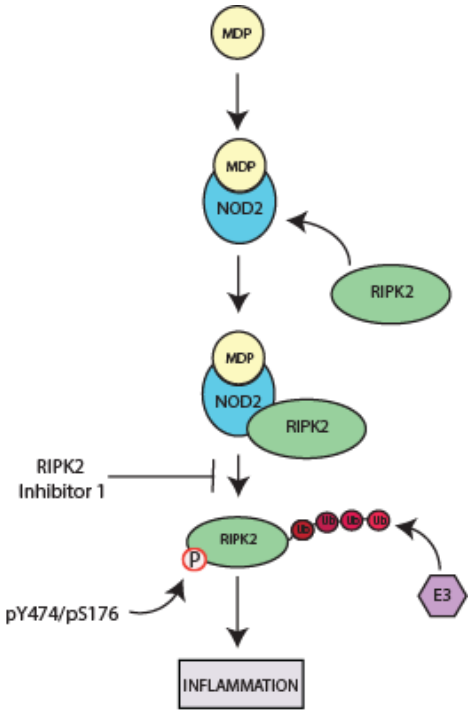

JPET Fast Forward. Published on March 19, 2018 as DOI: 10.1124/jpet.117.247163
This article has not been copyedited and formatted. The final version may differ from this version.

Introduction

Activation of NFκB proceeds through multiple pathways involving tumor necrosis factor receptor 1 (TNF-R1) and pathogen recognition receptors (PRRs) such as Toll like receptors (TLR) (Hayden and Ghosh, 2004; Madrid and Baldwin, 2003; Orlowski and Baldwin, 2002) and NOD2, an intracellular pattern recognition receptor. NOD2 is mainly stimulated by muramyl dipeptide (MDP), a bacterial product found in both Gram positive and negative bacteria, and requires the obligate kinase, RIPK2, to promote both NFκB activation and an autophagic response (Tigno-Aranjuez et al., 2010). Mice with genetic deletion of the *Nod2/Ripk2* have a dysbiotic intestinal flora resulting in altered susceptibility to intestinal inflammation (Ermann et al., 2014). In addition, the loss of *Ripk2* has been demonstrated to result in the inability of cells to carry out mitophagy leading to enhanced mitochondrial production of superoxide/reactive oxygen species and accumulation of damaged mitochondria that will trigger a caspase 1 dependent inflammasome activation.(Lupfer et al., 2014) In the context of malignant transformation, knockdown of RIPK2 down-regulated mRNA expression of E-cadherin and vimentin, both of which are involved in epithelial to mesenchymal transition (EMT) and metastatic promotion (Wu et al., 2012). RIPK2 might thus play an important role in cell migration (Wu et al., 2012) metastasis (Wu et al., 2012) and offer alternate novel therapeutics for abnormal inflammation driven by the NOD2/RIPK2 pathway.

Most RIPK2 inhibitors were not designed to inhibit RIPK2 and, thus, RIPK2 inhibition was an off target effect of the use of these drugs. These included Geftinib/Iressa (IC_{50} at 50 nM) (Canning et al., 2015), Regorafenib and other protein tyrosine kinases (Canning et al., 2015). Tigno-Aranjuez *et al*. published on the identification of novel class of RIPK2 inhibitors (OD36 and OD38) that can inhibit 92% kinase activity of RIPK2 at 100 nM and can alleviate inflammation in a rodent model for inflammatory bowel disease. However, like most RIPK2 inhibitors, at 100 nM, > 80% inhibition of Fyn, TGFB2, ALK-2, and Lck was also observed. WEHI-435, a recently characterized small molecule RIPK2 inhibitor was demonstrated to delay RIPK2 ubiquitination and NFκB activation downstream of NOD2 activation. In addition, WEHI-435 interfered with cytokine production *in vitro* and *in vivo* and ameliorates experimental autoimmune encephalomyelitis in mice (Nachbur et al., 2015). Recently, GlaxoSmithKline isolated a RIPK2 inhibitor, GSK-583, based on using the full RIPK2 protein to screen a DNA encoded library collection with a fluorescence polarization based binding assay as a readout (Haile et al., 2016). This bound to the ATP binding pocket of the kinase domain and inhibited RIPK2 with an IC_{50} of (5 – 50 nM) depending on the assay. Lastly, Novartis recently published on their RIPK2 inhibitor

JPET Fast Forward. Published on March 19, 2018 as DOI: 10.1124/jpet.117.247163
This article has not been copyedited and formatted. The final version may differ from this version.

obtained by virtual screening of their proprietary library that can inhibit RIPK2 with an IC_{50} of 3 nM (He et al., 2017). No *in vivo* applicability was analyzed but it can selectively inhibit MDP-promoted cytokine production in peripheral blood mononuclear cells and bone marrow derived mouse macrophages. A kinome analysis was not carried out and thus it is unknown if significant off target effects exist in the presence of the Novartis RIPK2 inhibitor.

Because of robust off target effects of most RIPK2 inhibitors, we carried out molecular modeling (docking) and cheminformatics analyses by carefully analyzing the only known crystal structure of RIPK2 in association with the c-ABL kinase inhibitor, ponatinib[1] (Canning and Bullock). Utilizing this structure, we searched chemical databases for scaffolds exerting significant binding interactions similar (or stronger) to those exerted by ponatinib, determined by comparing their free energies when docked inside of the RIPK2 binding site. In addition to RIPK2 binding as part of this computer-based (initial) screening, we selected compounds that inhibited EGFR (IC_{50}'s > 1000 nM; weak inhibitory activity) along with weak binding interactions in the EGFR and c-ABL binding sites, two common off-targets for previously identified RIPK2 inhibitors. Several hits are shown in Figure 1 and Table 1 and these compounds have unknown biological features. Since RIPK2 signals downstream of NOD2 and is linked to NFκB and autophagy activation, we speculate that the *in vivo* use of our selective RIPK2 inhibitors will target NFκB activation and possibly resolve abnormal inflammation states.

METHODS

Additional methods can be found in the Supplementary Experimental Procedures online.

Pharmacophore Search. Commercially available subsets of the ZINC (15,868,179 compounds) and MolPort (7,241,662 compounds) databases were screened using the lead drug ponatinib as a reference. We used the ZINCPharmer pharmacophore search server (Koes and Camacho, 2012) and pharmacophore features were identified directly from the RIPK2 structure (PDB ID: 4C8B) and used for the screening. In this regard, a total of 74 compounds were selected from both databases. The selected compounds were then docked into the RIPK2 binding site.

Structure Similarity Search. The PubChem (Kim et al., 2016) compound library (more than 80 million molecules) was compared to Ponatinib, to filter all molecules which are at least 60% similar to this compound (10,655,787 molecules). We selected the most (≥ 90%; 803 compounds) and less (< 62%; 50,000 compounds randomly selected from a total of

JPET Fast Forward. Published on March 19, 2018 as DOI: 10.1124/jpet.117.247163
This article has not been copyedited and formatted. The final version may differ from this version.

2,607,266) similar structures employing the PubChem Fingerprint (PCFP) implemented in the ChemmineR package (Cao et al., 2008) of the R program (R Development Group, 2008). The filtered compounds were then subjected to another filtering step based on the Lipinski's rule of five (Lipinski et al., 2001) removing the duplicates and inorganic molecules with the FAFDrugs3 server (Lagorce et al., 2015) (22,274 compounds). Finally, a total of 3,000 compounds were selected and optimized using the *obminimize tool* of the OpenBabel toolbox (O'Boyle et al., 2011) for the docking studies.

Molecular Docking. The crystal structure of the human RIPK2 (PDB: 4C8B) (Canning and Bullock) was retrieved from the Protein Data Bank (PDB) (Bernstein et al., 1977). Some residues in the three-dimensional structures were missing, and consequently, these side chain atoms were added using the WHAT IF Web Interface.(Vriend, 1990) The protein was subjected to an energy minimization employing the AMBER99SB force field by 1000-step steepest-descent minimization followed by 100-conjugate gradient minimization using UCSF CHIMERA v1.9 software (Pettersen et al., 2004). Polar hydrogens, Gasteiger-Marsili empirical atomic partial charges and the AutoDock atom types were computed employing the MGLTools v1.5.4 package (Morris et al., 2009). The torsional root and branches of the ligands were chosen with the same program, allowing flexibility for all rotational bonds (except for the amide bond). In addition, the software was used to assign Gasteiger-Marsili atomic charges to all ligands (Gasteiger et al. 1978). Docking calculations were performed using the AutoDock Vina software (Trott and Olson, 2010). A grid box of 28 $Å^3$ and centered at the binding site was used to calculate the atom types needed for the calculation. A total of 9 runs were performed with an exhaustiveness of 50. The best binding mode of each molecule was selected based on the lowest binding free energy score. The 3D figures were generated using PyMOL Molecular Graphics System (DeLano Scientific LLC, Palo Alto, CA, 2007) .

RIPK2 *In Vitro* Kinase Assay. For this protocol, samples were lysed in 1X RIPK2 lysis buffer (50 mM Tris, pH 7.5, `0 mM $MgCl_2$, 1% Triton X-100, 1 mM DTT, 1 mM EDTA, 1 mM EGTA, with freshly added 1 mM β-glycerophosphate and protease inhibitors [PMSF and aprotinin]) and immunoprecipitated overnight using 1.5 µg rabbit anti-RIPK2 antibody. The next day, protein G sepharose was used to immunoprecipitate the RIPK2 protein complex IP for 1.5 hours. Following this incubation, samples were washed once in 1 X kinase wash buffer (50 mM Tris, pH 7.5, 150 mM NaCl, 1% Trition X-100, 1 mM EDTA) followed by 2 washes with 1 X Kinase buffer (30 mM Hepes, pH 7.5, 10 mM $MgCl_2$, 2 mM $MnCl_2$). After last wash, 20 µl water was added to beads, followed by 1 X Kinase buffer and ^{32}P-γ-ATP and kinase

JPET Fast Forward. Published on March 19, 2018 as DOI: 10.1124/jpet.117.247163
This article has not been copyedited and formatted. The final version may differ from this version.

reaction was allowed to proceed for 45-60 minutes at 30 ^{o}C. Protein loading dye was added to the mix and samples were boiled and separated on an SDS-PAGE gel. The gel was dried and then exposed to X-ray film to capture the autophosphorylation of RIPK2.

NFκB Gene Reporter Luciferase Assay. Dual-Luciferase Reporter Assay System (DLR assay system, Promega, E1910) was used to perform dual-reporter assays on NFκB Luciferase and Renilla Luciferase (internal control). Briefly, HCT116 colon cancer cells were equally seeded at a density of 3 x 10^4 in 6-well plates and allowed to attach for 24 hrs. Prior to transfection, cells were washed with serum free media 3 times. Dual transfection was carried out using 12 μl of PEI to 3 μg of NFκB Luciferase construct and 60 ng of Renilla Luciferase construct. After 24 hours after transfection, cells were treated with the different drugs for 24-36 hrs. Cells were then lysed using the passive lysis buffer provided by the kit for 30 minutes on ice. Lysate was spun down for 8 minutes at 10,000 rpm and 20 μl of cell lysate were transferred in 96-well plate. Luciferase assays were analyzed based on ratio of Firefly/Renilla to normalize cell number and transfection efficiency.

Intestinal Inflammation Injury Model. Animals were administered 3% w/v DSS (molecular weight of 40 000 – 50 000, MP Biomedicals) in the drinking water for 7 days followed by recovery for 7 days. They were monitored for: piloerection, bloatednesss, tremors, lack of movement, rectal bleeding and weight loss (all on a scale of 0–5 with 5 being very severe, adapted from Madsen et. al, 2001). Animals were euthanized once rectal bleeding became grossly apparent. For weight loss, a score of 0 for no weight loss, 1 if 5% loss, 2 for 5– 10% loss, 3 for 10 – 15% loss, 4 for 15 – 20% loss and a score of 5 for > 20% loss in initial body weight. Disease activity indices (DAI) were the sum of all individual scores. All animals were male of the C57BL/6 background and at 10 – 12 weeks of age or 25 g in body weight at the beginning of the experiment.

Lung Inflammation Model. Male Balb/c mice (6-8 weeks) were sensitized on days 1 and 6 via intraperitoneal injection of 0.9% sterile saline (0.5 mL) or 0.9% saline containing 10 μg ovalbumin and 2 mg Al(OH)3. After light anesthesia with ketamine (75 mg/kg) and acepromazine (2.5 mg/kg), mice were challenged intranasally with 25 μl of saline containing 50 μg ovalbumin or saline alone as control on days 12 and 14. RIPK2 inhibitor -1 (1 μg/g body weight) or 30% DMSO

JPET Fast Forward. Published on March 19, 2018 as DOI: 10.1124/jpet.117.247163
This article has not been copyedited and formatted. The final version may differ from this version.

(solvent control for drug) were injected intraperitoneally on day 12, 13 and 14 (on day 12 and 14 the injection was performed 1 hr before the intranasal challenge with ovalbumin). On day 15, mice were euthanized with an intraperitoneal injection of 2 mg sodium pentobarbital. Cardiac puncture was used to collect blood, followed by tracheal intubation with polyethylene tubing. The lungs were washed twice, with 1 mL of phosphate buffered saline (PBS), pH 7.4, and the 2 mL of broncho-alveolar lavage (BAL) fluid was collected. BAL fluid was spun at 300 g for 5 min. Cell pellets were resuspended in PBS, total cell count was performed and then cytospins were prepared with 5000 cells. The slides were stained with Diff Quick and differential cells counts were done to assess allergic airway inflammation. This was done in collaboration with Dr. Harissios Vliagoftis (University of Alberta).

Mass Spectrometry. Direct-infusion measurements were carried out on an LTQ Orbitrap XL (Thermo Scientific) mass spectrometer using the Ion Max ESI source. The on board syringe pump was used with a 100uL Hamilton syringe and a flow rate of 5uL/min. The following parameters were used: sheath gas flow of 15 arbitrary units, auxiliary gas flow of 5 arbitrary units, spray voltage of 3.5 kV, tube lens voltage of 110 V, capillary temperature of 275C, capillary voltage of 35V, capillary temperature of 275 °C. The AGC target was set to 1e6 and the maximum injection time to 200 ms. The resolution was set at 100000 and two microscans were recorded.

NMR Spectroscopy. NMR experiments were run on a Varian Inova 500 MHz spectrometer at 30°C. The proton chemical shifts were measured relative to the residual protonated methyl (CHD_2) signal of d_6-DMSO (2.50 ppm); coupling constants (J) are reported in Hertz (Hz). Standard notation is used to describe the multiplicity of signals observed in 1H NMR spectra: singlet (s), doublet (d), triplet (t), broad (b) etc. Through-space and through-bond connectivities were observed using 2D ^{1}H-^{1}H ROESY experiment (mixing time 200 ms).[1] One-dimensional experiments were processed using VNMRJ (Varian Associates) and 2D ^{1}H-^{1}H ROESY was processed using NMRPipe/NMRDraw software.[2] RIPK2 inhibitor 1 was prepared by dissolving 0.3 mg in 500 µL d_6-DMSO. RIPK2 inhibitor 2 was prepared by dissolving 0.3 mg in 500 µL d_6-DMSO (Delaglio et al., 1995).

JPET Fast Forward. Published on March 19, 2018 as DOI: 10.1124/jpet.117.247163
This article has not been copyedited and formatted. The final version may differ from this version.

Use of animals. All animal experimentation was performed in accordance with University of Alberta institutional guidelines as defined by Animal Care and Use Committee.

Statistical analysis. This is carried out by ANOVA and Student's t-test (two-tailed) as indicated.

Results

Pharmacophore search

The ponatinib/RIPK2 complex (PDB: 4C8B) has revealed significant binding interactions of this inhibitor in the RIPK2 active site. Based on this crystal structure, the active site is localized in a binding pocket formed by at least eight different amino acid residues including Val32, Lys47, Glu66, Ile69, Leu70, Thr95, Met98, and Asp164 (Figure 1A). In this work, the ZINC and MolPort databases were screened with the ZINCPharmer pharmacophore search server using the lead drug Ponatinib as query. Several pharmacophoric features were identified directly from the RIPK2 structure and used for the screening. In this regard, a total of 74 compounds were identified from both databases with similar pharmacophoric points to ponatinib (Figure 1B). The compounds were then docked into the same RIPK2 binding site that in which ponatinib is located. Interestingly, 54 compounds shared the pharmacophore distribution of ponatinib. Table 1 summarizes the docking scores of the compounds with the lowest binding free energies. Figure 1B shows the location of the pharmacophoric points identified for the interaction of ponatinib with the RIPK2 active site and the proposed binding modes of the ligands with the lowest binding free energies, respectively. It is noteworthy that the compounds with the lowest calculated binding free energies exhibit a high structural similarity between them (MolPort-016-359-762 [labelled as RIPK2 inhibitor 1 in subsequent Figures, 3-benzamido-4-methyl-N-[3-(1-methyl-1H-imidazol-2yl)phenyl] benzamide], MolPort-015-752-252, MolPort-015-604-588, and MolPort-016-412-727) and a high correlation with pharmacophoric points of ponatinib. These results suggest that compound MolPort-016-359-762 and its derivatives have high probability to inhibit RIPK2.

Structure similarity search

A total of 10,655,787 compounds with at least 60% of similarity to ponatinib were obtained from the PubChem database to dock them into this binding site and identify new potential inhibitors. We selected the most (≥ 90%; 803 compounds) and less (< 62%; 50,000 compounds randomly selected from a total of 2,607,266) similar structures in order to identify

JPET Fast Forward. Published on March 19, 2018 as DOI: 10.1124/jpet.117.247163
This article has not been copyedited and formatted. The final version may differ from this version.

ponatinib-like molecules and novel scaffolds, respectively. After filtering with Lipinski's rule and removing duplicates and inorganic molecules, we performed molecular docking studies in the RIPK2 active site using AutoDock Vina, from which more than 500 compounds with a calculated ΔGbind ≤ -10.0 kcal/mol were identified. The docking scores of ponatinib and the compounds with the lowest binding free energies are summarized in Table 1. As might be expected, the compounds with the highest similarity values showed similar binding modes compared to ponatinib (PC_24826801, PC_57405602, PC_58945635, PC_58945682, PC_58945685). However, compound PC_57410628 was the only molecule with a lower binding free energy than the lead molecule. Moreover, compound PC_44716361 (MolPort-001-746-327 [labelled as RIPK2 inhibitor 2 in subsequent Figures]), which presents a lower similarity to ponatinib, represents a new scaffold with unique structural features offering alternatives from a Medicinal Chemistry perspective. Figure 1B shows the proposed binding mode of these ligands in the RIPK2 binding site. This figure also shows that all the compounds identified possible form hydrogen bonds between the Glu66 residue and the carboxamide group. The initial virtual screening ranking, chemical structures and the Pan Assay Interference Compounds (PAINS) (Sterling and Irwin, 2015) check of the selected compounds are reported in Supplemental Table 1.

Utilizing mass spectrometry and ^{1}H-NMR (Figure 2 and Supplemental Figures 1, 2, and 3A), we confirmed > 95% purity of our two lead compounds and confirmed structure of the identified RIPK2 inhibitors 1 and 2. ROESY (rotating-frame Overhauser enhancement spectroscopy) spectra provided through-bond and through-space connectivities that were essential for obtaining complete chemical shift assignments of both molecules (Supplemental Figures 1 and 2). In addition, through-space ROE (rotating-frame nuclear Overhauser enhancement) connectivities provided valuable information about the conformational preferences of RIPK2 inhibitor 1 in solution (Figure 2B). The lack of ROEs between HN22 and either HC17 or HC25 indicates that the central methyl-containing aromatic ring is roughly perpendicular to the amide plane of HN22, as would be expected based on steric considerations. In contrast, HN13 shows ROEs to HC8, HC17, and HC21, indicating that the two central benzene rings are more planar with respect to the central amide bond of HN13, similar to the conformation seen in ponatinib (Figure 1B). Thus, the arrangement of benzene rings found in RIPK2 inhibitor 1 resembles the geometry of the corresponding aromatic rings in ponatinib bound to RIPK2. The presence of both HN13-HC17 and HN13-HC21 ROEs suggest rotation about the C14-C16 bond, with rotomer i (Supplemental Figure 1B) matching the conformation found in ponatinib-RIPK2. However, the presence of an HN13-HC8 ROE coupled with the absence of an HN13-CH10 ROE suggests that rotation about the C9-N13 bond is more

JPET Fast Forward. Published on March 19, 2018 as DOI: 10.1124/jpet.117.247163
This article has not been copyedited and formatted. The final version may differ from this version.

restricted, which may force the imidazole ring of RIPK2 inhibitor 1 into a position opposite to the corresponding CF_3 group of ponatinib-RIPK2 (Figure 1B-iii), which would place it in a more solvent-exposed position than the buried position of the CF_3 group. Further detailed analysis may be warranted to isolate these two forms and determine bioactivities for RIPK2 and NFκB inhibition.

Validation of RIPK2 Inhibitors using Kinome Analysis

The specificity of the identified RIPK2 inhibitors to inhibit numerous kinases was explored utilizing the Kinome Scan profiling service at DiscoverX. This utilizes an *in vitro* kinase approach with purified recombinant kinases/peptide substrates to determine activity of kinases in the panel. We explored if our lead compounds, RIPK2 inhibitor 1 and 2, can inhibit other targets at 100 nM in the 97 kinome panel (Supplemental Table 2A). This concentration was utilized due to robust inhibition of NFκB and RIPK2 kinase assay in assays outlined in Figures 2-6. The kinome inhibition analysis revealed robust selectivity towards RIPK2 for RIPK2 inhibitor 1 with 20-27 % inhibition of c-ABL, Aurora kinase B or ERBB2 (Supplemental Table 2A). RIPK2 inhibitor 2 appears to inhibit 38% of the activity of SNARK and 27% of the activity of FGFR2, GSK3-β, JNK1, CSNK1G2 (Caesin kinase 1), and MET tyrosine kinase. These off target inhibitions are not surprising as it is difficult to obtain a specific small molecule inhibitor. It would suggest possible activities beyond inhibiting RIPK2 that will need to be empirically tested. Initial empirical testing for c-ABL was carried out via an *in vitro* kinase approach with purified recombinant kinases at the MRC Protein Phosphorylation and Ubiquitination Unit in Dundee, Scotland. Both our RIPK2 small molecule lead compounds inhibited c-ABL but with IC_{50} of > 100 μM (Figure 3A). Given this observation, we hope that the off target effects on Aurora kinase B and ERBB2 (if any) will also be in a vastly different concentration range of 100 nM.

Cell based Confirmation of RIPK2 Inhibition and Inhibition of NFκB Activation

We next explored cell based *in vitro* inhibition of RIPK2. We can clearly observe RIPK2 inhibitor 1 and 2 inhibition of MDP-dependent activation of RIPK2 autophosphorylation (on tyrosine 474) using an *in vitro* kinase assay in HCT116 cells (Figure 3B). MDP is the molecular ligand for the NOD2 pathogen receptor whereby RIPK2 can be activated. Similar results for RIPK2 inhibitor 1 inhibition of RIPK2 were obtained in breast cancer cells (BT549 and MDA-MB231 cells, data not shown). Immunodepeletion using an anti-RIPK2 antibody (Figure 3C, condition B) or Crispr/Cas9 knockout of

JPET Fast Forward. Published on March 19, 2018 as DOI: 10.1124/jpet.117.247163
This article has not been copyedited and formatted. The final version may differ from this version.

RIPK2 (Figure 3D) confirmed specificity of detection of the autophosphorylated RIPK2 band in Figure 3B. Furthermore, using a phospho-tyrosine [Y] 474 (in-house generated) and a phospho-serine [S] 176 (Cell Signaling, Inc.) RIPK2 antibodies, we confirmed that active RIPK2 is recognized by these antibodies upon activation with MDP treatment in 293HEK fibroblast and HCT116 colon cancer epithelial cells (Figure 3E, left panel) and detection of constitutively active RIPK2 in the colon cancer cell line, SW480 (Figure 3E, right panel). Interestingly, we can observe constitutively active RIPK2 in Hodgkin's Lymphoma cell lines HDMYZ, L428 (Figure 4A) and KMH2 cells (Figure 4B). This signal can effectively be inhibited using RIPK2 inhibitor 1, 2 and regorafenib (a known RIPK2 kinase inhibitor) at 100 nM as determined using RIPK2 phospho-specific antibodies (Figure 4A and B). Furthermore, we determined that RIPK2 inhibitor 1 effectively inhibited KHM2 cells at an approximate IC_{50} of 5 – 10 nM and kinase activity is somewhat sensitive to detergent conditions (Figure 4B and C). When compared to inhibition with ponatinib (a known RIPK2 inhibitor and chemical template for selecting our RIPK2 small molecule), our RIPK2 inhibitor performed equally to inhibit RIPK2 kinase activity in an *in vitro* kinase assay in two different cell lines (Figure 4D).

The functional consequence of inhibiting MDP-dependent activation of RIPK2 is the loss of NFκB activity (Figure 5A-C and Supplemental Figure 3B) and DNA binding ability, especially for the IL-8 promoter (Supplemental Figure 4A). Not surprisingly, RIPK2 inhibitor 1 was more efficacious at 100 nM at inhibiting NFκB activity when compared to RIPK2 inhibitor 2, gefitinib or regorafenib (p value comparing RIPK2 inhibitor 1 vs RIPK2 inhibitor 2 or gefitinib or regorafenib inhibition of MDP-driven NFκB activation was 0.0015, 0.0006 and 0.004 respectively). However, RIPK2 inhibitor 1 was as efficacious as ponatinib at 100 nM for NFκB inhibition (p value = 0.06 when comparing RIPK2 inhibitor 1 vs ponatinib inhibition of MDP-driven NFκB activation). Interestingly, a recently characterized RIPK2 inhibitor, GSK-583 (Haile et al., 2016) did not inhibit MDP-dependent NFκB activity at 100 nM in HCT116 cells (data not shown) although known to in primary immune cells. Interestingly, we did observe a small but significant reduction in LPS (via TLR4 and TLR2), TNFα, and IL-1β-dependent activation of NFκB (Figure 5C and an approximate IC_{50} in Figure 5D, Supplemental Figure 3B). Although a reduction, the approximate IC_{50} for RIPK2 inhibition of LPS-driven NFκB activation is > 20 μM and we speculate it will also be much higher for inhibition of TNFα, and IL-1β-dependent activation of NFκB. Interestingly, RIPK2 inhibitor 1 can also inhibit the activation of hypoxia response element I response to chemical induction using 1% H_2O_2 (Supplemental Figure 3C) to suggest either a link to inflammation or a

JPET Fast Forward. Published on March 19, 2018 as DOI: 10.1124/jpet.117.247163
This article has not been copyedited and formatted. The final version may differ from this version.

direct modulation of HIFα function. These observations validate the specificity of our RIPK2 inhibitor for NOD/RIPK2 biology and usefulness as an *in vivo* inhibitor of MDP-driven inflammation.

RIPK2 Inhibitors Can Inhibit the Proliferation of Several Cancer Cells but Do Not Promote Apoptosis or Cell Cycle Arrest

Inflammation is a strong driver of malignant transformation and abnormal proliferation, especially in colon (Lasry et al., 2016) and breast (Suman et al., 2016). We explored the ability of RIPK2 inhibitors to reduce the proliferative rate of highly metastatic cancer cells. For most of the cancer cells, 45-100 nM of RIPK2 inhibitor 1 inhibited > 70% of the proliferation of colon and blood cancer cells while preserving the proliferation of normal Rat-1 and ModeK intestinal epithelial cells (Figure 6A). These data would suggest strong suppressive properties of RIPK2 inhibitor 1 and to some extent inhibitor 2 on cell proliferation. Regorafenib, a recently characterized RIPK2 inhibitor, did not significantly inhibit the proliferation of these cells in an MTT assay (Figure 6A). We also observed inhibition of triple negative breast cancer cells, HCT1143 and MDA-MB231, with RIPK2 inhibitor 1 (Supplemental Figure 4B) to suggest effective anti-proliferative properties. The approximate IC_{50} for inhibition was around 30-60 nM for most of the cells tested (two are shown in Supplemental Figure 4C). This effect on growth inhibition was not due to alterations in cell cycle (Supplemental Figure 5) nor a significant increase in the apoptotic cell populations to suggest that RIPK2 inhibition of proliferation is independent of cell cycle or apoptotic changes.

RIPK2 Inhibitors Do Not Inhibit RIP1 Directed Cell Death, Ferroptosis or Modulation of Mitochondrial Physiology

The RIPK family of proteins are actively involved in numerous cell death processes beyond death receptor dependent cell death (Vanden Berghe et al., 2016). We characterized two forms of cell death involving erastin stimulated ferrroptosis (an iron dependent form of cell death, Supplemental Figure 6A) and VAD-fmk (Z), Smac Mimetic-164 (S) and TNFα (T) (ZST) stimulation of RIPK1-directed cell death (Supplemental Figure 6B). In both cases, RIPK2 inhibitor 1 did not interfere with these forms of cell death to support our cell cycle effects and to suggest no overlap with RIPK1 biology (Supplemental Figure 6A). Recently, RIPK3 was demonstrated to require Bax/Bak effect on the mitochondrial permeability transition pore (MPTP) in order to carry out necroptosis and the importance of both RIPK1 and RIPK3 in

JPET Fast Forward. Published on March 19, 2018 as DOI: 10.1124/jpet.117.247163
This article has not been copyedited and formatted. The final version may differ from this version.

relation to necroptosis-directed degenerative, inflammatory and infectious diseases has been published (Moriwaki et al., 2015). We thus explored how the identified RIPK2 inhibitors can perturb mitochondrial physiology by evaluating the activity of the sirtuins, a class of deacetylases that use NAD^+ to remove acetyl groups from proteins.(Tang, 2016) Indeed, the putative SIRT1 activator, resveratrol, can stimulate mitochondrial biogenesis to promote increased wellness in the individual (Ostojic, 2017). We, therefore, explored the effect on Sirtuin activity using the BIOMOL assay as described previously (Dai et al., 2016). We can observe no statistically significant increase in SIRT1 activation when using the compounds at 0.1 or 10 μM, indicating that phenotypes observed for the use of RIPK2 inhibitors at these doses in cells are likely through SIRT1-independent mechanisms when compared to the effect of resveratrol (Supplemental Figure 6C). The identified RIPK2 inhibitors are thus selective inhibitors of RIPK2-dependent NFκB pathways if we consider the data in Figure 5 and Supplemental Figures 3B, 4 and 5.

RIPK2 Inhibitors Can Efficiently Resolve Intestinal Inflammation in an Ulcerative Colitis Model

DSS-induced intestinal inflammation is a model for ulcerative colitis (UC, a form of inflammatory bowel disease, IBD). DSS functions to irritate the colonic mucosa to promote localized inflammation, active cell death and localized destruction of the epithelial barrier to the lumen of the colon (Dieleman et al., 1998). These events subsequently drive inflammation damage indicative of what IBD patients encounter. NOD2 mutations have been observed in IBD patients lending support for dysregulated NOD2/RIPK2 signaling driving inflammation in IBD patients (Branquinho et al., 2016). We have demonstrated the importance of *R*as *ass*ociation domain *f*amily protein *1A,* RASSF1A (or 1A), in the pathogenesis of colitis in a rodent model (Gordon et al., 2013). RASSF1A is a tumor suppressor involved in TNF-R1 dependent apoptosis, cell cycle control and restriction of NFκB activation (Gordon et al., 2013). The *Rassf1a* knockout mice (both heterozygous and homozygous forms) are very susceptible to DSS-induced inflammation injury (Gordon et al., 2013) mainly due to uncontrolled inflammation linked to the NOD2/RIPK2 pathway (Said et al, unpublished observation).

We, therefore, carried out intraperitoneal injection of 1 μg/g body weight of RIPK2 inhibitor 1 or 2 on day 5, 7, and 9 to offset the pre-inflammation damage stage, peak inflammation damage stage and post-inflammation damage/restitution phase. Using this treatment scheme, we observed a robust difference on day 9 in the disease activity indices of wild type and *Rassf1a* knockout mice that was significantly inhibited with the use of the RIPK2 inhibitors, especially RIPK2 inhibitor 1 (Figure 6B and Table 2). Interestingly, a newly characterized RIPK2 inhibitor, gefitinib, can

JPET Fast Forward. Published on March 19, 2018 as DOI: 10.1124/jpet.117.247163
This article has not been copyedited and formatted. The final version may differ from this version.

also inhibit intestinal inflammation injury but only promote a 41% survival vs 73% survival with RIPK2 inhibitor 1 (Figure 6B and Table 2). Similar results were obtained for the protein tyrosine kinase inhibitor, regorafenib (data not shown). Since both gefitinib and our RIPK2 inhibitors can inhibit RIPK2, either our drug has more affinity for RIPK2 or the off target effects of RIPK2 inhibitor 1 is beneficial to aid in recovery from inflammation injury using the DSS model.

We then explored pharmacokinetic properties of RIPK2 inhibitor 1 in the sera of mice. Analysis revealed that RIPK2 Inhibitor 1 can be eluted at ~3.7 minutes in a region of the chromatogram free of interfering substances (Supplemental Figure 6D, top panel). After a dose of 1-2 mg/kg IP of inhibitor, the compound was not quantifiable in mouse serum. However, after dosing mice with 15 mg/kg IP, the RIPK2 inhibitor was of measurable concentrations in most of the serum samples assayed. The mean C_{max} was 114 ng/mL occurring at 1 h after dosing, and the area under the serum concentration versus time curve was 573 ng×h/mL, with a terminal phase half-life of 1.9 h being observed. Therefore, it appears that RIPK2 inhibitor 1 may be efficiently metabolized within 2 hours and cleared from the blood (Supplemental Figure 6D, bottom panel). Furthermore, toxicity analysis carried out 9 days after the last dose of intraperitoneal injection of 2 μg/g body weight revealed little or no changes in > 98% of the markers characterized in a complete blood count (Supplemental Figure 7). However, creatine kinase activity was significantly elevated in animals treated with RIPK2 inhibitor 1 as opposed to RIPK2 inhibitor 2. During treatment with RIPK2 inhibitor 1 (and post-treatment) we did not overtly observe phenotypic changes in these animals nor noticed evidence of health conditions to support a creatine kinase abnormality (such as skeletal muscle defect and movement abnormalities or unexpected euthanasia due to a cardiac abnormality). Interestingly, it has been shown that the creatine/phosphocreatine pathway may play a central role in energy metabolism and nutritional creatine supplementation has been shown to impart beneficial effects in a number of diverse disease pathologies (Kitzenberg et al., 2016). We speculate this to be the case as resetting of metabolic abnormalities is needed for recovery of IBD patients that have metabolic syndrome disorder (Goncalves et al., 2015). Further analysis is required to determine if elevated creatine kinase is affecting the health of the animal, how sustained it is and if it can be alleviated with RIPK2 inhibitor 1 analogs. In addition, detail analysis is needed on how our RIPK2 inhibitor 1 is metabolized, removed from the blood, where it accumulates or if it can cross the blood-brain barrier. These are all unanswered questions that we are currently addressing.

JPET Fast Forward. Published on March 19, 2018 as DOI: 10.1124/jpet.117.247163
This article has not been copyedited and formatted. The final version may differ from this version.

RIPK2 Inhibitors Can Also Efficiently Resolve Lung Inflammation in an Asthma Model

RIPK2 has also been implicated in allergic airway inflammation. RIPK2 gene silencing in the airways decreased allergic airway inflammation in an ovalbumin-mediated mouse model of asthma (Jun et al., 2013). Furthermore, an association between a RIPK2 promoter polymorphism and childhood severe asthma has been shown in a Japanese population (Nakashima et al., 2006). Since we can observe robust inhibition of NFκB in the presence of RIPK2 inhibitor 1 and a > 70% recovery of animals from DSS-induced inflammation injury (Figure 4 and 6B), we proceeded to explore ability to resolve lung inflammation using the ovalbumin challenge model (Kumar et al., 2008). Ovalbumin elicits a robust inflammatory reaction in the airways characterized by increased number of total cells and eosinophils in the bronchoalveolar lavage (BAL) of ovalbumin sensitized mice (Figure 6B). In the presence of RIPK2 inhibitor 1 (and to some extent with RIPK2 inhibitor 2), we observed a significant reduction in both total cell numbers and eosinophil numbers in BAL fluid. This data suggest effective inhibition of lung inflammation.

Discussion

RIPK2 is the obligate kinase to the NOD2 pathogen receptor pathway and has been demonstrated to be involved in NFκB activation and metastatic behaviour in some cancers (Jun et al., 2013) and has a distinct activity versus RIPK1, 3 or 4 (Chirieleison et al., 2016). In addition, several reports suggest involvement in the activation of the immune response upon viral infection (Lupfer et al., 2013) and the requirement for the NOD2/RIPK2 molecular pathway in several models on inflammatory diseases including experimental colitis (Branquinho et al., 2016) and arthritis (Vieira et al., 2012). Colorectal cancer (CRC) is only one example of a disease that can arise from a prior state of persistent or chronic inflammation. Individuals with IBD and primary sclerosing cholangitis (inflammation of the bile ducts) are at a much higher risk for progressing to CRC and require closer management of their debilitating disease (Dyson and Rutter, 2012; Williamson and Chapman, 2015). As such, therapies to modulate and control inflammation are robust cancer prevention strategies.

Herein, we performed pharmacophore and similarity-based search and molecular docking studies toward the identification of potential novel RIPK2 inhibitors. In the pharmacophore search we identified several molecules that share the pharmacophore arrangement with ponatinib. From these, compound MolPort-016-359-762 is one of the most attractive molecules to be tested since it exhibits a high correlation with the pharmacophore model and lowest binding free

JPET Fast Forward. Published on March 19, 2018 as DOI: 10.1124/jpet.117.247163
This article has not been copyedited and formatted. The final version may differ from this version.

energy (highest score). Moreover, the similarity-based virtual screening predicted ten molecules as new potential RIPK2 inhibitors. The lower docking score of one of the less similar compounds MolPort-001-746-327 present more attractive scaffold to be repositioned as inhibitors of this enzyme. Interestingly, several analogs of MolPort-016-359-762 also showed higher affinities for the active site pocket of RIPK2, suggesting a high preference of this scaffold for the active site pocket. These analogs may even afford a greater selectivity to inhibit RIPK2 (data not shown). We are currently exploring the use of these analogs of MolPort-016-359-762.

As mentioned earlier, several RIPK2 inhibitors have been characterized. However, like most RIPK2 inhibitors, at 100 nM, OD36 and OD38 can also inhibit Fyn, TGFβ2, ALK-2, and Lck by > 80%. Our identified RIPK2 inhibitors reveal lower binding free energies that other RIPK2 inhibitors identified suggesting that our inhibitor may be more active. Furthermore, our identified RIPK2 inhibitors appear to have more affinity for the active site of RIPK2 than others, more efficacious at inhibition of proliferation and can effectively resolve lung inflammation and intestinal inflammation more robustly than gefitinib (Figure 6B and Table 2). The efficacious quality of RIPK2 inhibitor 1 in resolving intestinal inflammation may arise from the fact that it can have a small but significant effect on TNFα, IL-1β and LPS driven NFκB activation as seen in Figure 5 and Supplemental Figure 3B. Most inflammatory diseases are complex diseases that have a multitude of inflammatory pathways targeting the area. Thus, to effectively resolve inflammation in these areas, a broad spectrum inhibitor may be needed to target multiple TLRs and pathogen receptors.(Murgueitio et al., 2017)

All of our *in vivo* inhibition was at 1 - 2 μg/g body weight, which is much lower than the level used for most small molecules inhibitor. Preliminary pharmacokinetics suggest a 1.89 hour half-life in the blood (Supplemental Figure 6D) and chronic experiments using RIPK2 inhibitor 1 agree with our preliminary pharmacokinetics to suggest the efficacious quality of this inhibitor can last for up to 5-6 days after a 1 -2 μg/g body weight intraperitoneal injection (data not shown). We are currently completing our pharmacokinetic analysis and will be exploring inhibition of intestinal inflammation in the *IL-10*$^{-/-}$ model for inflammatory bowel disease, a model with spontaneous colonic inflammation by 8-10 weeks of age and an established model for IBD (Kuhn et al., 1993).

It has been demonstrated by several groups that RIPK2 has a unique requirement for NOD1 and NOD2 and functions in many pathways different from RIPK1, 3 or 4. Recently, Chirieleison *et al.* (2016) summarized the uniqueness of RIPK2 kinase domain within the RIPK family that could not be substitute for the kinase domain from RIPK1 or RIPK4. Indeed, RIPK2 inhibitors 1 and 2 did not inhibit RIPK1 biology nor ferroptosis, a form of cell death influenced by

JPET Fast Forward. Published on March 19, 2018 as DOI: 10.1124/jpet.117.247163
This article has not been copyedited and formatted. The final version may differ from this version.

proteins of the RIPK family (Supplemental Figures 6A and B). As such, we believe that our identified RIPK2 inhibitor 1 and 2 can selectively modulate RIPK2 specific biology in agreement with the observations of Chirieleison *et al.* (2016).

Although we can observe a robust inhibition of autophosphorylation of RIPK2, NFκB and alleviation of intestinal and airway inflammation injury in our mouse models of colitis and asthma, our kinome screen demonstrated *in vitro* inhibition of several other kinases including 20-30% inhibition of c-ABL, Aurora kinase B or ERBB2. We have demonstrated importance of c-ABL in driving inflammation injury in our acute DSS model in the publication of Gordon et al. (2013). It is likely that our RIPK2 inhibitor 1 may interfere with the kinase activity of these off targets indirectly by resolving the inflammation. Many of these kinases are involved in growth related pathways, tumorigenesis pathways and cell cycle control such as Aurora Kinase B (Borisa and Bhatt, 2017). These off target effects may actually be beneficial in treating IBD, PSC, PSC/IBD-related CRC and asthma whereby a multitude of abnormal signaling involving inflammation, oxidative damage, DNA damage and apoptotic abnormalities exist to manifest itself into a diseased state. Thus, eliminating all of these abnormalities using a single small molecule will promote a return to homeostasis and recovery from inflammation damage. It will be interesting to explore other inflammation states such as obesity, diabetes, cystic fibrosis, psoriasis and arthritis to determine the importance of RIPK2 in driving inflammation damage and the usefulness of RIPK2 inhibitor 1 to alleviate the clinical symptoms associated with these diseases.

Comparison with Recently Identified RIPK2 Inhibitors

Recently, four inhibitors to RIPK2 were identified as OD36/OD38 (Tigno-Aranjuez et al., 2014) WEHI-435 (Nachbur et al., 2015), GSK-583 (Haile et al., 2016) and the one from Novartis (He et al., 2017). OD36 and OD38 were obtained through a small molecule macrocylization process from Oncodesign. IC_{50} values of < 100 nM and the ability to interfere with MDP dependent RIPK2 activity. WEHI-435 was obtained by analysis of the RIPK2/ponatinb structure and the necrostatin-1/murine RIPK1 structure to obtain a structural face for the murine RIPK2 kinase domain (18-249) (Nachbur et al., 2015). Using this structural face, the utilized computational biology to obtain small molecules to associate with the RIPK2 ATP-binding pocket, GSK-583 was obtained using structural comparisons of RIPK2 with ponatinib. Lastly, the Novartis RIPK2 inhibitor was obtained in a similar manner to GSK583 and was based on a proprietary chemical library screen. Several hits were obtained and after structural optimization a RIPK2 inhibitor was obtained to inhibit RIPK2 kinase activity at 3 nM (He et al., 2017).

JPET Fast Forward. Published on March 19, 2018 as DOI: 10.1124/jpet.117.247163
This article has not been copyedited and formatted. The final version may differ from this version.

In this study, we utilized similarity-based virtual screening and molecular docking analysis to identify a RIPK2 inhibitor that can empirically inhibit the autophosphorylation of RIPK2, inhibit NFκB and alleviate lung and intestinal inflammation efficacious at 1-2 μg/g body weight. RIPK2 Inhibitors did not inhibit RIPK1 activity involved in ferroptosis or cell death nor have an effect on mitochondrial biology. In addition, RIPK2 inhibitor 1 appears to also inhibit cell proliferation as determined by MTT assay that does not appear to be promoting cell death. We find this curious and will be further exploring how RIPK2 inhibitors 1 and 2 can promote reduced proliferation and interfere with inflammation. Interestingly, RIPK2 has been demonstrated to be involved the active growth of CD90(+) intestinal stromal cells to suggest an "inflammatory" cross talk between intestinal stromal cells and the epithelial cells (Owens et al., 2013) and we can observe robust activation of RIPK2 in IBD colon tissue sections immunostained with our proprietary pY474 RIPK2 antibody (Salla *et al.,* unpublished observations). Inflammation signals from stromal cells and the epithelial cells will drive abnormal states to produce a cytokine storm that fuels malignant growth. Inhibitors to RIPK2 may have promising therapeutic potential to uniquely interfere with NFκB-dependent biology and offer an alternative to existing anti-inflammatory therapies.

ACKNOWLEDGMENTS

We thank all the members of the Baksh laboratory for their helpful discussions.

AUTHOR CONTRIBUTIONS

Conducted experiments: M.S, R.A.O, D.G.I, A.Z, A.S, A. R. B., S.F, R.M V.P, K.S.B, Y.F, J. M. and S.B.

Participated in research design; M.S, R.A.O, I.S.G, C.V.M, H.V, D.B, B.P.H and S.B.

Performed data analysis: M.S, R.A.O, P.H, , J. M., A. R. B., L.R.G, P.M and S.B.

Wrote or contributed to the writing of the manuscript: M.S, R.A.O and S.B.

References

Bernstein, F.C., Koetzle, T.F., Williams, G.J., Meyer, E.E., Brice, M.D., Rodgers, J.R., Kennard, O., Shimanouchi, T., and Tasumi, M. (1977). The Protein Data Bank: a computer-based archival file for macromolecular structures. Journal of molecular biology *122*, 535.

Borisa, A.C., and Bhatt, H.G. (2017). A comprehensive review on Aurora kinase: Small molecule inhibitors and clinical trial studies. European journal of medicinal chemistry *140*, 1-19.

Branquinho, D., Freire, P., and Sofia, C. (2016). NOD2 mutations and colorectal cancer - Where do we stand? World journal of gastrointestinal surgery *8*, 284-293.

Canning, P., and Bullock, A. Structure of the kinase domain of human RIPK2 in complex with ponatinib. To be Published.

Canning, P., Ruan, Q., Schwerd, T., Hrdinka, M., Maki, J.L., Saleh, D., Suebsuwong, C., Ray, S., Brennan, P.E., Cuny, G.D., *et al.* (2015). Inflammatory Signaling by NOD-RIPK2 Is Inhibited by Clinically Relevant Type II Kinase Inhibitors. Chemistry & biology *22*, 1174-1184.

Cao, Y., Charisi, A., Cheng, L.C., Jiang, T., and Girke, T. (2008). ChemmineR: a compound mining framework for R. Bioinformatics *24*, 1733-1734.

Chirieleison, S.M., Kertesy, S.B., and Abbott, D.W. (2016). Synthetic Biology Reveals the Uniqueness of the RIP Kinase Domain. Journal of immunology *196*, 4291-4297.

Dai, H., Ellis, J.L., Sinclair, D.A., and Hubbard, B.P. (2016). Synthesis and Assay of SIRT1-Activating Compounds. Methods Enzymol *574*, 213-244.

Delaglio, F., Grzesiek, S., Vuister, G.W., Zhu, G., Pfeifer, J., and Bax, A. (1995). NMRPipe: a multidimensional spectral processing system based on UNIX pipes. Journal of biomolecular NMR *6*, 277-293.

Dieleman, L.A., Palmen, M.J., Akol, H., Bloemena, E., Pena, A.S., Meuwissen, S.G., and Van Rees, E.P. (1998). Chronic experimental colitis induced by dextran sulphate sodium (DSS) is characterized by Th1 and Th2 cytokines. Clinical and experimental immunology *114*, 385-391.

Dyson, J.K., and Rutter, M.D. (2012). Colorectal cancer in inflammatory bowel disease: what is the real magnitude of the risk? World journal of gastroenterology *18*, 3839-3848.

Ermann, J., Staton, T., Glickman, J.N., de Waal Malefyt, R., and Glimcher, L.H. (2014). Nod/Ripk2 signaling in dendritic cells activates IL-17A-secreting innate lymphoid cells and drives colitis in T-bet-/-.Rag2-/- (TRUC) mice. Proceedings of the National Academy of Sciences of the United States of America *111*, E2559-2566.

Goncalves, P., Magro, F., and Martel, F. (2015). Metabolic inflammation in inflammatory bowel disease: crosstalk between adipose tissue and bowel. Inflammatory bowel diseases *21*, 453-467.

Gordon, M., El-Kalla, M., Zhao, Y., Fiteih, Y., Law, J., Volodko, N., Anwar-Mohamed, A., El-Kadi, A.O., Liu, L., Odenbach, J.*, et al.* (2013). The tumor suppressor gene, RASSF1A, is essential for protection against inflammation -induced injury. PloS one *8*, e75483.

Haile, P.A., Votta, B.J., Marquis, R.W., Bury, M.J., Mehlmann, J.F., Singhaus, R., Jr., Charnley, A.K., Lakdawala, A.S., Convery, M.A., Lipshutz, D.B.*, et al.* (2016). The Identification and Pharmacological Characterization of 6-(tert-

Butylsulfonyl)-N-(5-fluoro-1H-indazol-3-yl)quinolin-4-amine (GSK583), a Highly Potent and Selective Inhibitor of RIP2 Kinase. Journal of medicinal chemistry *59*, 4867-4880.

Hayden, M.S., and Ghosh, S. (2004). Signaling to NF-kappaB. Genes & development *18*, 2195-2224.

He, X., Da Ros, S., Nelson, J., Zhu, X., Jiang, T., Okram, B., Jiang, S., Michellys, P.Y., Iskandar, M., Espinola, S.*, et al.* (2017). Identification of Potent and Selective RIPK2 Inhibitors for the Treatment of Inflammatory Diseases. ACS medicinal chemistry letters *8*, 1048-1053.

Jun, J.C., Cominelli, F., and Abbott, D.W. (2013). RIP2 activity in inflammatory disease and implications for novel therapeutics. Journal of leukocyte biology *94*, 927-932.

Kim, S., Thiessen, P.A., Bolton, E.E., Chen, J., Fu, G., Gindulyte, A., Han, L., He, J., He, S., Shoemaker, B.A.*, et al.* (2016). PubChem Substance and Compound databases. Nucleic Acids Res *44*, D1202-1213.

Kitzenberg, D., Colgan, S.P., and Glover, L.E. (2016). Creatine kinase in ischemic and inflammatory disorders. Clinical and translational medicine *5*, 31.

Kuhn, R., Lohler, J., Rennick, D., Rajewsky, K., and Muller, W. (1993). Interleukin-10-deficient mice develop chronic enterocolitis. Cell *75*, 263-274.

Kumar, R.K., Herbert, C., and Foster, P.S. (2008). The "classical" ovalbumin challenge model of asthma in mice. Current drug targets *9*, 485-494.

Lagorce, D., Sperandio, O., Baell, J.B., Miteva, M.A., and Villoutreix, B.O. (2015). FAF-Drugs3: a web server for compound property calculation and chemical library design. Nucleic Acids Res *43*, W200-207.

Lasry, A., Zinger, A., and Ben-Neriah, Y. (2016). Inflammatory networks underlying colorectal cancer. Nature immunology *17*, 230-240.

Lipinski, C.A., Lombardo, F., Dominy, B.W., and Feeney, P.J. (2001). Experimental and computational approaches to estimate solubility and permeability in drug discovery and development settings. Advanced drug delivery reviews *46*, 3-26.

Lupfer, C., Thomas, P.G., Anand, P.K., Vogel, P., Milasta, S., Martinez, J., Huang, G., Green, M., Kundu, M., Chi, H.*, et al.* (2013). Receptor interacting protein kinase 2-mediated mitophagy regulates inflammasome activation during virus infection. Nature immunology *14*, 480-488.

Lupfer, C.R., Anand, P.K., Liu, Z., Stokes, K.L., Vogel, P., Lamkanfi, M., and Kanneganti, T.D. (2014). Reactive oxygen species regulate caspase-11 expression and activation of the non-canonical NLRP3 inflammasome during enteric pathogen infection. PLoS pathogens *10*, e1004410.

Madrid, L.V., and Baldwin, A.S., Jr. (2003). Regulation of NF-kappaB by oncoproteins and tumor suppressor proteins. Methods in molecular biology *223*, 523-532.

Madsen, K., Cornish, A., Soper, P., McKaigney, C., Jijon, H., Yachimec, C., Doyle, J., Jewell, L., and De Simone, C. (2001). Probiotic bacteria enhance murine and human intestinal epithelial barrier function. Gastroenterology *121*, 580-591.

Moriwaki, K., Bertin, J., Gough, P.J., Orlowski, G.M., and Chan, F.K. (2015). Differential roles of RIPK1 and RIPK3 in TNF-induced necroptosis and chemotherapeutic agent-induced cell death. Cell death & disease *6*, e1636.

Morris, G.M., Huey, R., Lindstrom, W., Sanner, M.F., Belew, R.K., Goodsell, D.S., and Olson, A.J. (2009). AutoDock4 and AutoDockTools4: Automated docking with selective receptor flexibility. J Comput Chem *30*, 2785-2791.

Murgueitio, M.S., Rakers, C., Frank, A., and Wolber, G. (2017). Balancing Inflammation: Computational Design of Small-Molecule Toll-like Receptor Modulators. Trends in pharmacological sciences *38*, 155-168.

Nachbur, U., Stafford, C.A., Bankovacki, A., Zhan, Y., Lindqvist, L.M., Fiil, B.K., Khakham, Y., Ko, H.J., Sandow, J.J., Falk, H.*, et al.* (2015). A RIPK2 inhibitor delays NOD signalling events yet prevents inflammatory cytokine production. Nature communications *6*, 6442.

Nakashima, K., Hirota, T., Suzuki, Y., Akahoshi, M., Shimizu, M., Jodo, A., Doi, S., Fujita, K., Ebisawa, M., Yoshihara, S.*, et al.* (2006). Association of the RIP2 gene with childhood atopic asthma. Allergology international : official journal of the Japanese Society of Allergology *55*, 77-83.

O'Boyle, N.M., Banck, M., James, C.A., Morley, C., Vandermeersch, T., and Hutchison, G.R. (2011). Open Babel: An open chemical toolbox. Journal of cheminformatics *3*, 33.

Orlowski, R.Z., and Baldwin, A.S., Jr. (2002). NF-kappaB as a therapeutic target in cancer. Trends in molecular medicine *8*, 385-389.

Ostojic, S.M. (2017). Mitochondria-targeted nutraceuticals in sports medicine: a new perspective. Research in sports medicine *25*, 91-100.

Owens, B.M., Steevels, T.A., Dudek, M., Walcott, D., Sun, M.Y., Mayer, A., Allan, P., and Simmons, A. (2013). CD90(+) Stromal Cells are Non-Professional Innate Immune Effectors of the Human Colonic Mucosa. Frontiers in immunology *4*, 307.

Pettersen, E.F., Goddard, T.D., Huang, C.C., Couch, G.S., Greenblatt, D.M., Meng, E.C., and Ferrin, T.E. (2004). UCSF Chimera--a visualization system for exploratory research and analysis. J Comput Chem *25*, 1605-1612.

Sterling, T., and Irwin, J.J. (2015). ZINC 15--Ligand Discovery for Everyone. J Chem Inf Model *55*, 2324-2337.

Suman, S., Sharma, P.K., Rai, G., Mishra, S., Arora, D., Gupta, P., and Shukla, Y. (2016). Current perspectives of molecular pathways involved in chronic inflammation-mediated breast cancer. Biochemical and biophysical research communications *472*, 401-409.

Tang, B.L. (2016). Sirt1 and the Mitochondria. Molecules and cells *39*, 87-95.

Tigno-Aranjuez, J.T., Asara, J.M., and Abbott, D.W. (2010). Inhibition of RIP2's tyrosine kinase activity limits NOD2-driven cytokine responses. Genes & development *24*, 2666-2677.

Tigno-Aranjuez, J.T., Benderitter, P., Rombouts, F., Deroose, F., Bai, X., Mattioli, B., Cominelli, F., Pizarro, T.T., Hoflack, J., and Abbott, D.W. (2014). In vivo inhibition of RIPK2 kinase alleviates inflammatory disease. The Journal of biological chemistry *289*, 29651-29664.

Trott, O., and Olson, A.J. (2010). AutoDock Vina: improving the speed and accuracy of docking with a new scoring function, efficient optimization, and multithreading. J Comput Chem *31*, 455-461.

Vanden Berghe, T., Hassannia, B., and Vandenabeele, P. (2016). An outline of necrosome triggers. Cellular and molecular life sciences : CMLS *73*, 2137-2152.

Vieira, S.M., Cunha, T.M., Franca, R.F., Pinto, L.G., Talbot, J., Turato, W.M., Lemos, H.P., Lima, J.B., Verri, W.A., Jr., Almeida, S.C.*, et al.* (2012). Joint NOD2/RIPK2 signaling regulates IL-17 axis and contributes to the development of experimental arthritis. Journal of immunology *188*, 5116-5122.

Vriend, G. (1990). WHAT IF: a molecular modeling and drug design program. J Mol Graph *8*, 52-56, 29.

Williamson, K.D., and Chapman, R.W. (2015). Primary sclerosing cholangitis: a clinical update. British medical bulletin *114*, 53-64.

Wu, S., Kanda, T., Nakamoto, S., Imazeki, F., and Yokosuka, O. (2012). Knockdown of receptor-interacting serine/threonine protein kinase-2 (RIPK2) affects EMT-associated gene expression in human hepatoma cells. Anticancer research *32*, 3775-3783.

Footnotes:

1) Authors M. Salla and R.Aguayo-Ortiz contributed equally to this manuscript

The research in this study was supported by grants from Alberta Innovates – Health Solutions CRIO, Alberta Heritage Foundation for Medical Research, from the division of Hematology/Oncology/Palliative Care/ Epidemiology under Dr. David Eisenstat for funds to partially support this project and from the Stollery Children's Hospital and Stollery Children's Hospital/WCHRI Hair Massacure Donation Fund. Aguayo-Ortiz is very grateful to CONACyT (Mexico) for the fellowship granted (No. 510728/288862).

JPET Fast Forward. Published on March 19, 2018 as DOI: 10.1124/jpet.117.247163
This article has not been copyedited and formatted. The final version may differ from this version.

Figure legends

Figure 1 (A) Schematic of the RIPK2 active site. (B) Representation of pharmacophore points: hydrogen bond donor (HBD, yellow), hydrogen bond acceptor (HBA, orange), hydrophobic (Hyd, cyan) and aromatic (Ar, green). Predicted binding modes of (i) ponatinib (green), (ii) MolPort-016-359-762 (orange) and (iii) MolPort-016-412-727 (blue) in the RIPK2 binding site. (iv) Comparison between the binding position of ponatinib found within the crystal structure (yellow) and the binding mode predicted by AutoDock Vina (green). Predicted binding modes of (v) PC_57410628 (purple), PC_68349611 (brown), and (vi) PC_44716361 (MolPort-001-746-327, orange) in the RIPK2 binding site. All hydrogens were omitted for clarity. The dotted lines represent distances for the formation of hydrogen bonds.

Figure 2. Mass spectrometry and NMR confirmation of mass and structure of RIPK2 Inhibitor 1. (A) Direct-infusion measurements were carried out on an LTQ Orbitrap XL (Thermo Scientific) mass spectrometer using the Ion Max ESI source. Mass confirmation was obtained as indicated. (B) Two-dimensional ^{1}H-^{1}H ROESY spectrum of 3-benzamido-4-methyl-N-[3-(1-methyl-1H-imidazol-2-yl)phenyl]benzamide. Boxes (orange) represents through-space connectivities between protons in the compound. Blue boxes are signals due to 3-bond *J*-coupling between aromatic ring protons. 4-bond *J*-coupling signal is less intense.

Figure 3. Analysis of RIPK2 Kinase Activity. (A) Kinase activity for c-ABL was tested in the presence of inhibitor 1 and 2. IC_{50} for c-ABL for both inhibitors is > 100 μM. Analysis was carried out using purified c-ABL and the substrate peptide, EAIYAAPFAKKK, in association with the MRC Unit on Phosphorylation and Ubiquitination, University of Dundee, Scotland. (B) RIPK2 autophosphorylation at site Y474 is shown. Inhibition was carried out on cells followed by lysis and immunoprecipitation (IP) with rabbit anti-RIPK2 overnight. Following protein G pull down and wash, ^{32}P-γ-ATP is added and kinase reaction allowed to proceed for 30 minutes at 30 C. Following kinase reaction, SDS-PAGE was used to separate out the proteins, gel was then dried and exposed to film. (C) RIPK2 in HCT116 cells were IP with an anti-RIPK2 antibody (A) and the supernatant after IP in (A) was IP in (B) with the same RIPK2 antibody and in vitro kinase (IVK) assay carried out on both samples. (D) Crispr/Cas9 knockout of RIPK2 in HCT116 colon cells was carried out followed by MDP activation and RIPK2 IVK analysis. To illustrate use of RIPK2 Crispr/Cas9 reagents and specificity

JPET Fast Forward. Published on March 19, 2018 as DOI: 10.1124/jpet.117.247163
This article has not been copyedited and formatted. The final version may differ from this version.

of our IVK assay. (E) Left panel, Cells were stimulated with MDP for 3 hours and RIPK2 activation was monitored by a phosphotyrosine (pY) 474 RIPK2 antibody (in house antibody) and phosphoserine (pS)176 phosphorylation (Cell Signaling). Right panel, several colon cancer cells were investigated for constitutive activation of RIPK2 using phosphorylation specific antibodies to pY474 and pS176 as indicated. Bottom, constitutive activation of RIPK2 in numerous cell lines are explored.

Figure 4. Characterization of RIPK2 kinase Inhibitors. (A) Immunoblot illustration of the use of RIPK2 phospho-antibodies in two Hodgkin's lymphoma cells that have constitutive active RIPK2. A comparison with a known RIPK2 inhibitor is shown (regorafenib). All inhibitor concentrations were 100 nM. Similar results were observed for a third Hodgkin's lymphoma cell line, KMH2 (see B). (B) KMH2 Hodgkin's lymphoma cells were inhibited *in vivo* for 33-36 hours using the indicated concentration of RIPK2 inhibitor 1. Top, an *in vitro* kinase assay was carried out by IP overnight with 1 μg of the rabbit-anti RIPK2 antibody from ProteinTech and 1 ml of lysate form a confluent 6 well dish of KMH2 cells. Immune complexes were separated by SDS-PAGE and captured by autoradiography. Bottom, quantitation of 3-5 independent experiments to reveal an approximate IC_{50} of 5 – 10 nM for *in vivo* RIPK2 inhibition. (C) Analysis of effect of drug solvent (DMSO), salt concentration and detergents on the kinase activity of RIPK2. Following IP, the indicated reagents were added for 10 minutes followed by 32-γ-ATP to initiate the kinase reaction as described in Experimental Section (D) RIPK2 *in vitro* kinase assay was carried out as in Fig, 3B in KMH2 and HCT116 cells in the presence of ponatinib or RIPK2 inhibitor 1 in order to carry out a comparison of RIPK2 inhibition.

Figure 5. RIPK2 Inhibition of NFκB Activity. (A-B) NFκB gene reporter assay determination of inhibition of MDP stimulated NFκB activity with RIPK2 inhibitors (A) and an approximate IC_{50} determination for inhibition of MDP driven-NFκB activation using RIPK2 inhibitors 1 and 2 (B). All drugs in (A) were utilized at 100 nM. P values for RIPK inhibitor treated vs MDP (no drug) = < 0.0001 (inhibitor 1), 0.06 for inhibitor 2, < 0.006 (Gefitinib), 0.0002 (Regorafinib), and 0.0008 (Ponatinib). For ponatinib, n = 4 and n = 10 for the rest with approximate IC_{50} curves shown in (B). (C) Left panel, NFκB gene reporter assay determination of inhibition of LPS stimpulated NFκB activity with RIPK2 inhibitors (concentration as indicated). P values for RIPK2 inhibitor treated vs LPS (no drug) is < 0.02

JPET Fast Forward. Published on March 19, 2018 as DOI: 10.1124/jpet.117.247163
This article has not been copyedited and formatted. The final version may differ from this version.

(inhibitor 1) and < 0.268 (for inhibitor 2) (n = 6). Right panel, approximate IC_{50} determination for inhibition of LPS-NFκB driven inflammation using RIPK2 inhibitor 1 and 2 (B).

Figure 6. *In vivo* inhibition of proliferation, intestinal and lung inflammation using RIPK2 inhibitors. (A) RIPK2 Inhibitors modulate the proliferation of several colon cancers but not normal cells. MTT assay was carried out with the indicated concentrations of RIPK2 inhibitors in the indicated cell lines. HCT116 and DLD-1 are colon cancer cell lines while RAT-1 and MODEK are normal rat and mouse intestinal cell lines, respectively. RIPK2 inhibitor 1 does not appear to interfere with proliferation of normal intestinal cells (Rat-1 and ModeK) at 45 nM. For all experiments, n = 5 - 29. P value of HCT116 (+ inhibitor 1) versus HCT116 (+ inhibitor 2) was < 0.03; DLD-1 (+ inhibitor 1) versus DLD-1 (+ inhibitor 2) was < 0.02; DLD-1 (+ inhibitor 1) versus DLD-1 (+ Regorafenib) was < 0.006. For RIPK2 inhibitor 1 treated DLD-1 or HCT116 vs RIPK2 inhibitor 1 treated ModeK or Rat-1 cells (normal cells), p < 0.002 (analysis in either cell type); For RIPK2 inhibitor 2 treated DLD-1 or HCT116 vs RIPK2 inhibitor 2 treated ModeK cells (normal cells), p < 0.02 and 0.098 (analysis in DLD-1 or HCT116 cells respectively); for Regorafenib treated DLD-1 vs Regorafenib treated ModeK (normal cells), p < 0.2 but > 0.05. (B) Intestinal inflammation injury was carried out using the dextran sodium sulfate (DSS) model. DSS is taken up in the drinking water and migrates to the colon to cause irritation and localized inflammation. *Rassf1a*$^{-/-}$ mice are extremely sensitive to this model with < 25% survival following a 3% DSS insult for 7 days followed by water for 7 days. Most *Rassf1a*$^{-/-}$ mice require euthanasia by day 7-9. Disease activity is scored based on rectal bleeding, piloerection, movement and body weight changes as described previously.(Madsen et al., 2001). N = 10 – 25 and p value of *Rassf1a*$^{-/-}$ (DSS) vs WT (DSS) was < 0.0001; *Rassf1a*$^{-/-}$ (DSS) vs *1a*$^{-/-}$ (DSS + inhibitor 1 or 2 or gefitinib) was < 0.0001. (C) *In vivo* inhibition of lung inflammation in an ovalbumin-induced asthma model in mice. Sensitization and challenge with ovalbumin in this model induces accumulation of inflammatory cells in the BAL that are primarily eosinophils. Administration of RIPK2 inhibitor-1 significantly decreased both the number of total cells and the number of eosinophils in the BAL fluid (n=8 for each group). P value for comparison between OVA alone and OVA+RIPK2 inhibitor-1 was 0.019 for total cell numbers and 0.003 for eosinophils. Please note that RIPK2 inhibitor 2 was not utilized in this experiment due to its higher approximate IC_{50} for NFκB (see Fig. 5B), (D) Model for disruption of NOD2/RIPK2 biology in the presence of RIPK2 inhibitor 1. RIPK2 is activated via tyrosine (Y) (pY474) and serine (S)

JPET Fast Forward. Published on March 19, 2018 as DOI: 10.1124/jpet.117.247163
This article has not been copyedited and formatted. The final version may differ from this version.

(pS176) phosphorylation and ubiquitination events to allow for associations with downstream components. RIPK2 inhibitor 1 inhibits phosphorylation at serine 176 and tyrosine 474 and possible inhibition of ubiquitination of RIPK2.

SUPPLEMENTAL INFORMATION

Supplemental Information includes Supplemental table and Figures which can be found online.

JPET Fast Forward. Published on March 19, 2018 as DOI: 10.1124/jpet.117.247163
This article has not been copyedited and formatted. The final version may differ from this version.

Table 1. Calculated binding free energies of potential RIPK2 inhibitors. ZINC, MolPort and PubChem (PC) molecule identification numbers are shown. MolPort-016-359-762 is RIPK2 inhibitor 1 and PC_44716361 (MolPort-001-746-327) is RIPK2 inhibitor 2.

Search method	Compound	ΔG_{bind} (kcal/mol)	Compound	ΔG_{bind} (kcal/mol)
Pharmacophore	Ponatinib	-11.9	MolPort-015-604-588	-10.6
	MolPort-016-359-762	-11.5	MolPort-016-412-727	-10.6
	MolPort-015-752-252	-10.8	ZINC02739307	-10.1
Structure similarity	PC_57410628	-12.0	PC_58945682	-11.5
	PC_44716361	-11.8	PC_58945685	-11.5
	PC_24826801	-11.8	PC_68349611	-11.5
	PC_57405602	-11.6	PC_58945669	-11.3
	PC_58945635	-11.6	PC_40780119	-11.1

JPET Fast Forward. Published on March 19, 2018 as DOI: 10.1124/jpet.117.247163
This article has not been copyedited and formatted. The final version may differ from this version.

Table 2. Survival of *Rassf1a*$^{-/-}$ animals during DSS-induced inflammation. The presence of RIPK2 inhibitors reduced acute intestinal inflammation and enhanced overall survival of the mice.

RIPK2 Inhibitor	Treatment and Genotype	Percent Survival
No Drug	DSS-treated *Rassf1a*$^{-/-}$	7/30 = 22%
1 (MolPort-016-359-762)	DSS-treated *Rassf1a*$^{-/-}$	8/11 = 73 %
2 (MolPort-001-746-327)	DSS-treated *Rassf1a*$^{-/-}$	5/9 = 56 %
Gefitinib	DSS-treated *Rassf1a*$^{-/-}$	7/15 = 47 %

JPET Fast Forward. Published on March 19, 2018 as DOI: 10.1124/jpet.117.247163
This article has not been copyedited and formatted. The final version may differ from this version.

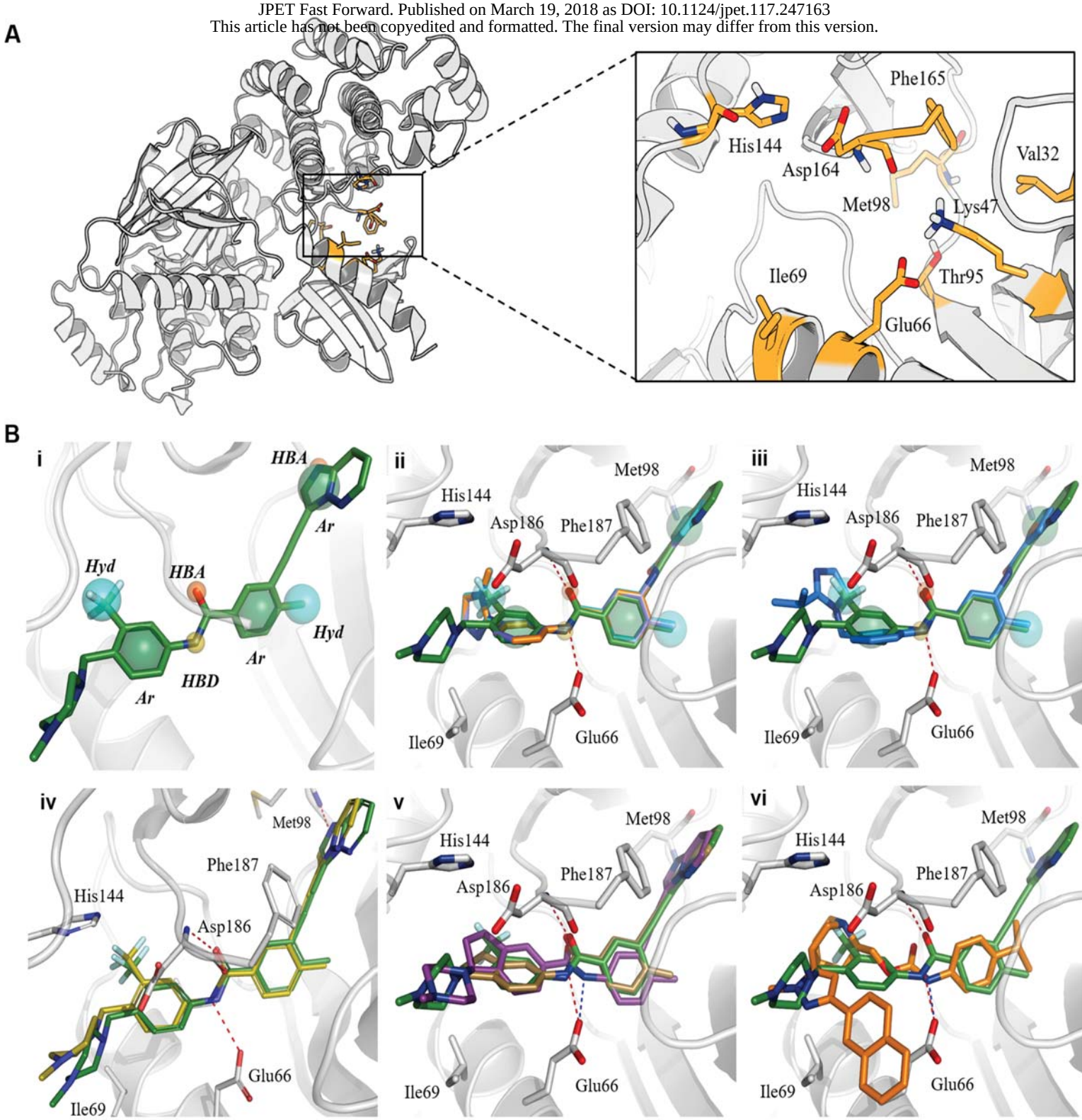

Salla et al, Figure 1

JPET Fast Forward. Published on March 19, 2018 as DOI: 10.1124/jpet.117.247163
This article has not been copyedited and formatted. The final version may differ from this version.

A

Mass Spectrometry Confirmation of RIPK2 Inhibitor 1 Formula Weight

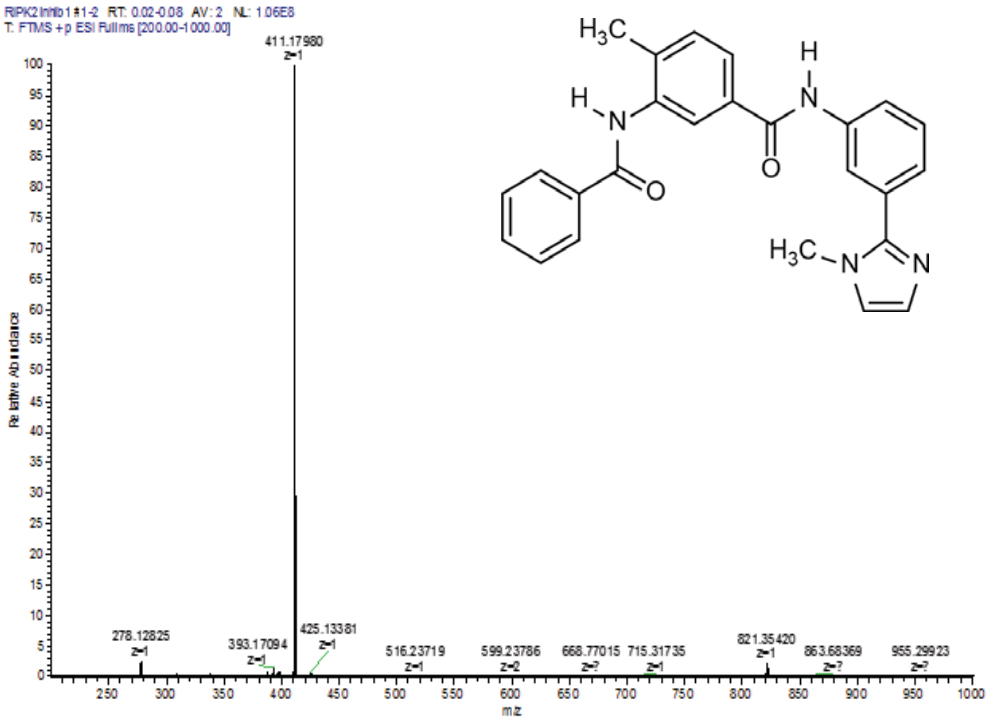

B

RIPK2 Inhibitor 1 - Two Dimensional 1H-1H ROESY Spectrum

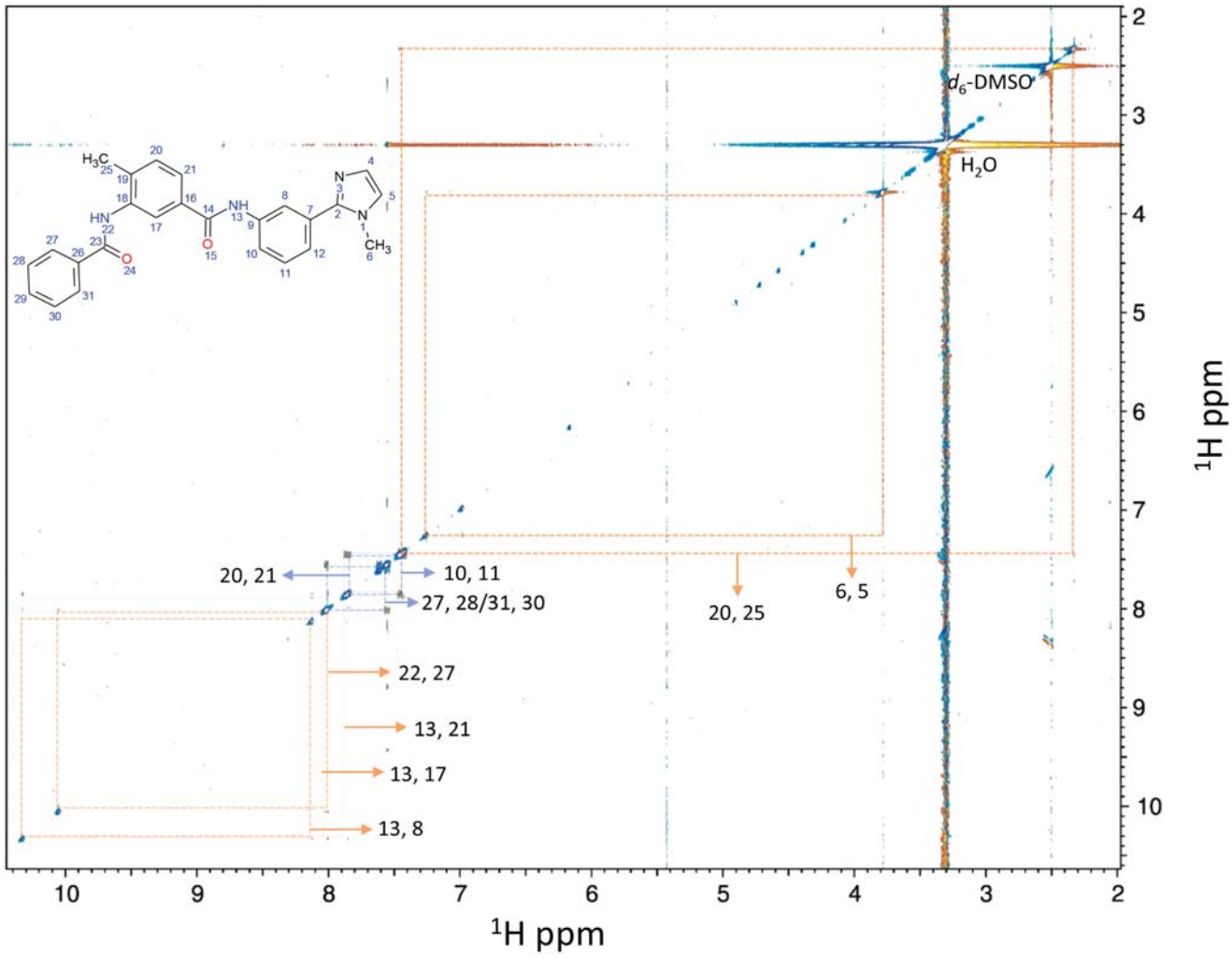

JPET Fast Forward. Published on March 19, 2018 as DOI: 10.1124/jpet.117.247163
This article has not been copyedited and formatted. The final version may differ from this version.

A

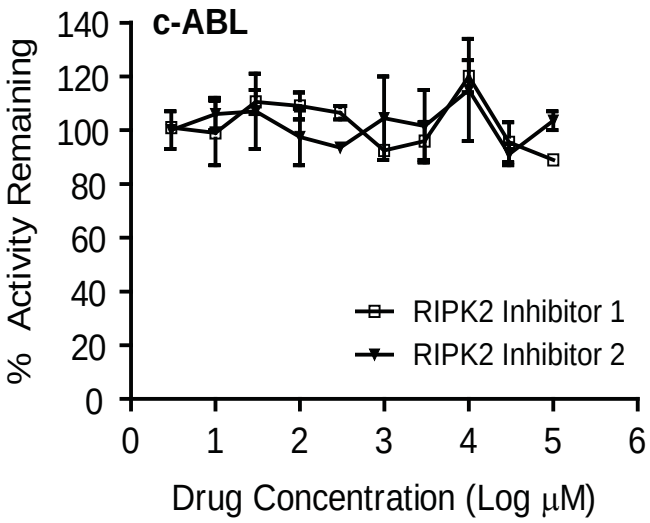

B

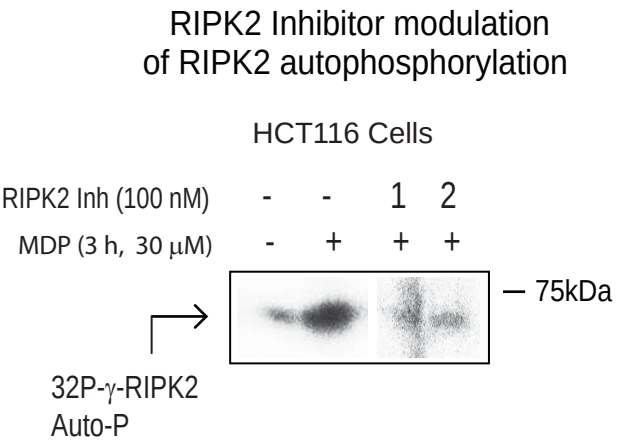

C

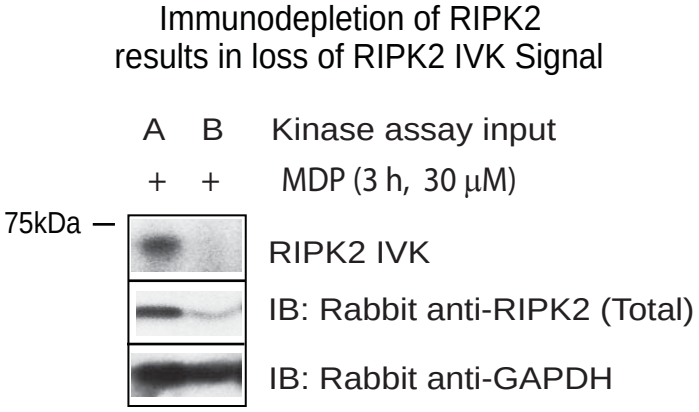

D

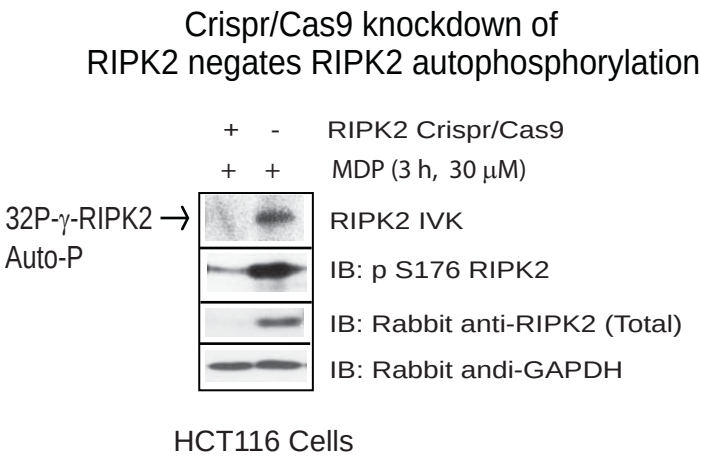

E

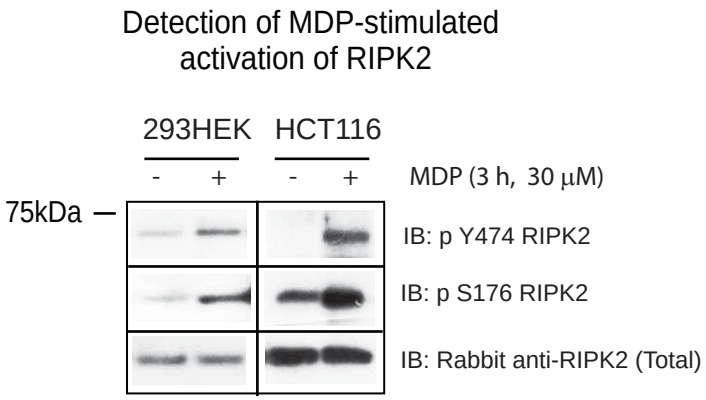

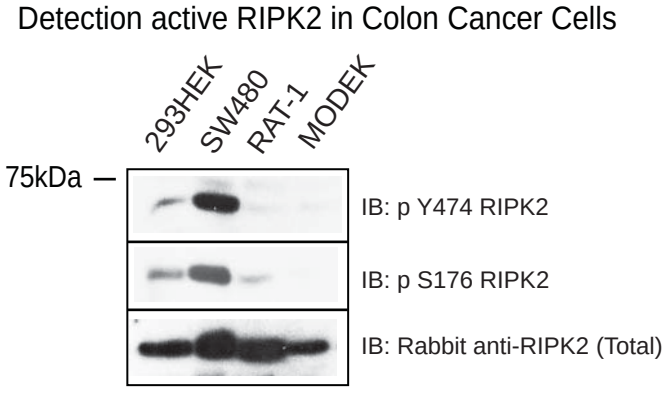

JPET Fast Forward. Published on March 19, 2018 as DOI: 10.1124/jpet.117.247163
This article has not been copyedited and formatted. The final version may differ from this version.

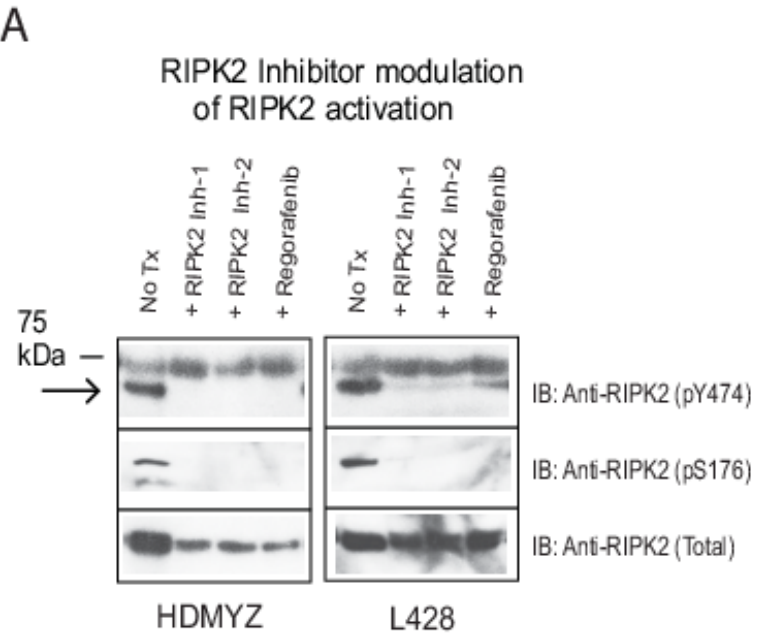

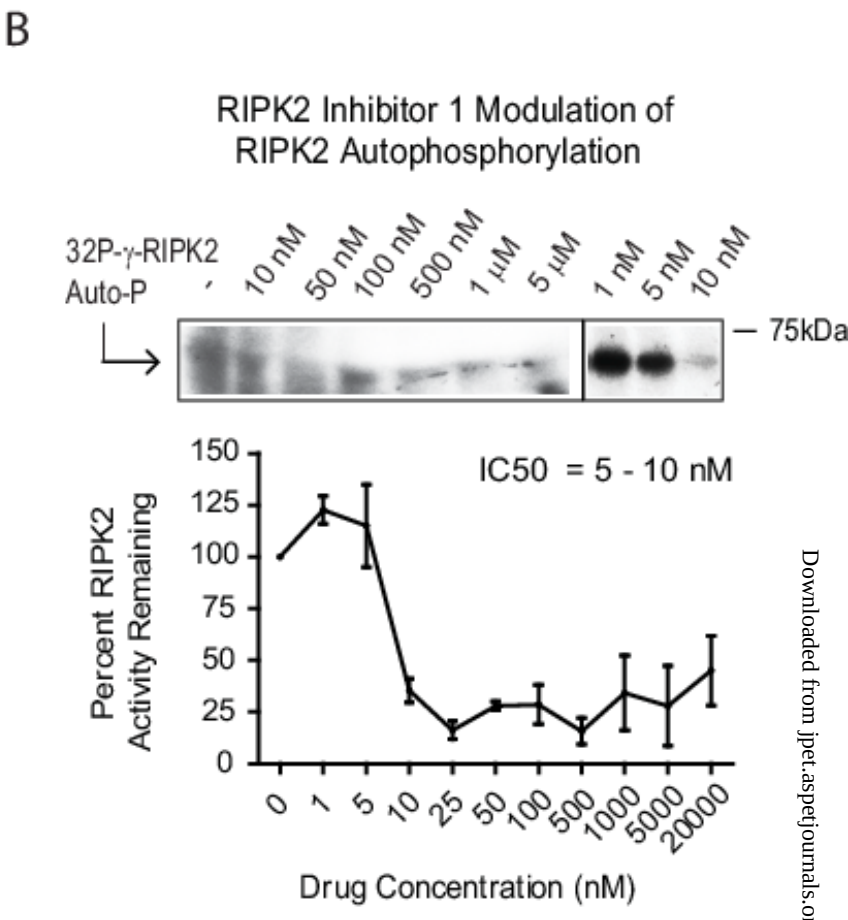

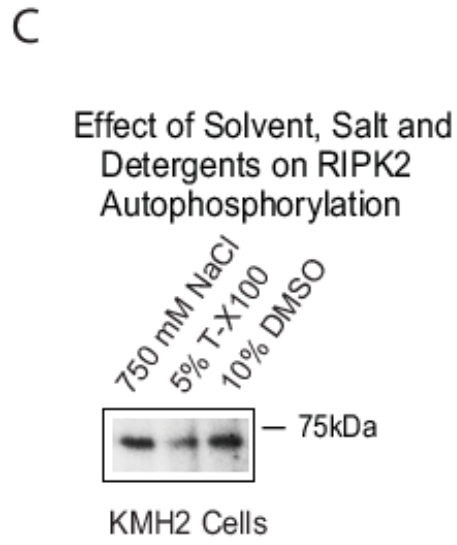

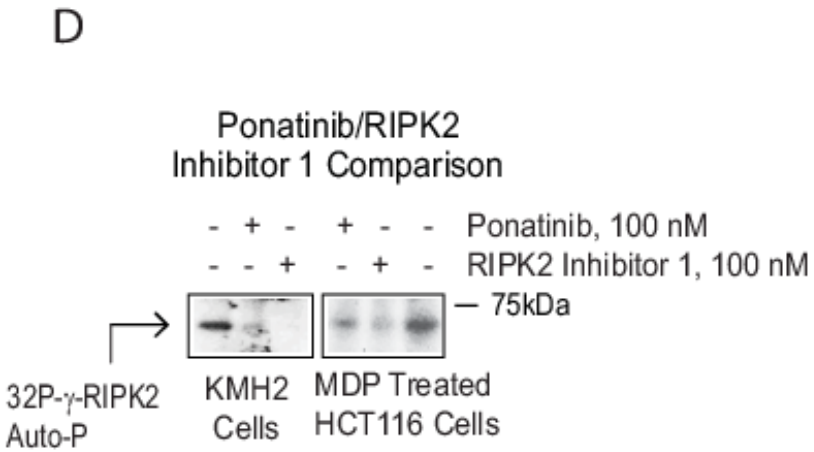

JPET Fast Forward. Published on March 19, 2018 as DOI: 10.1124/jpet.117.247163
This article has not been copyedited and formatted. The final version may differ from this version.

A

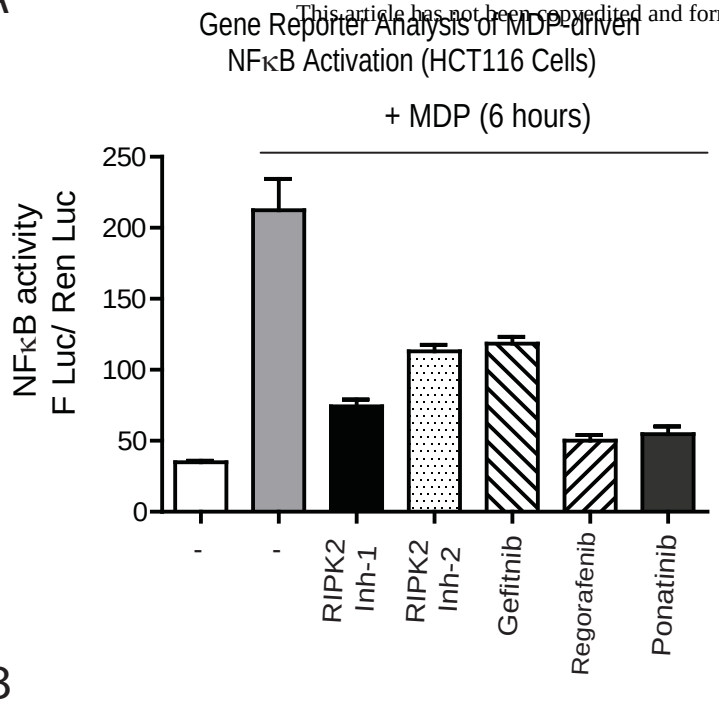

B

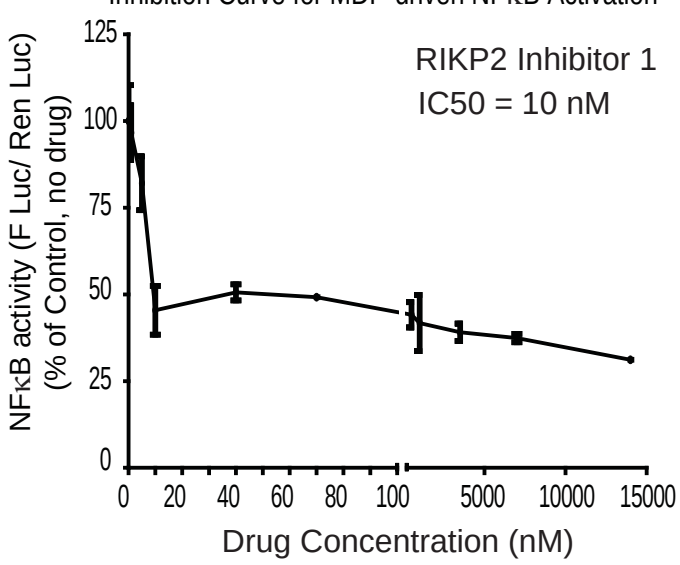

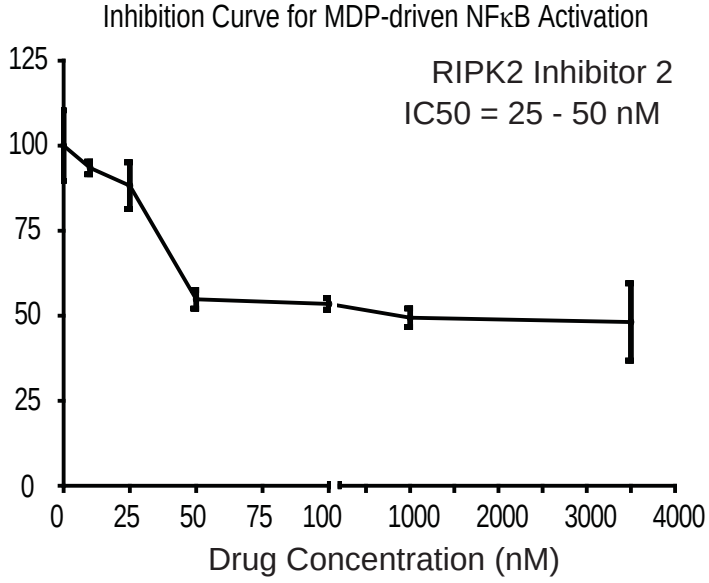

C

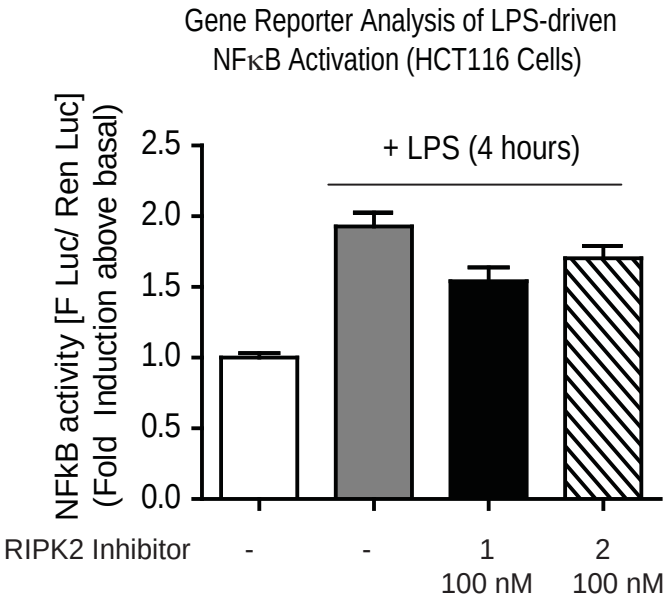

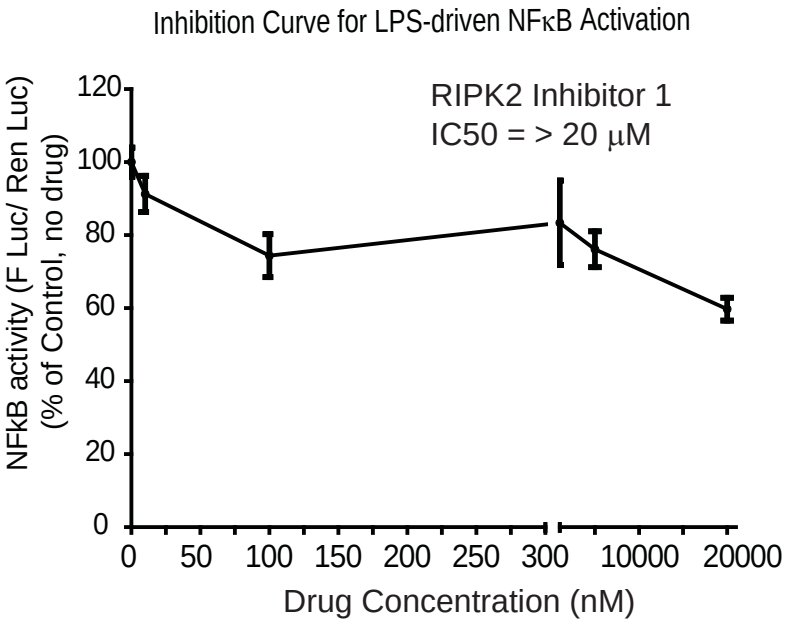

JPET Fast Forward. Published on March 19, 2018 as DOI: 10.1124/jpet.117.247163
This article has not been copyedited and formatted. The final version may differ from this version.

A

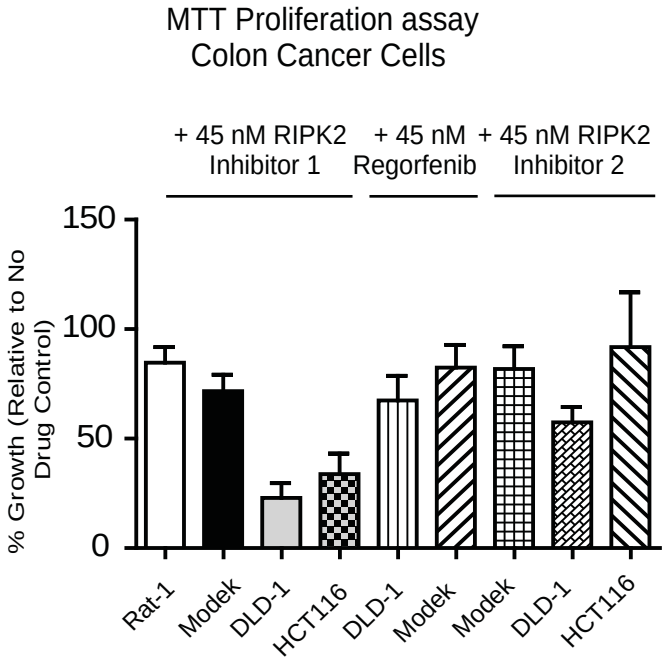

B

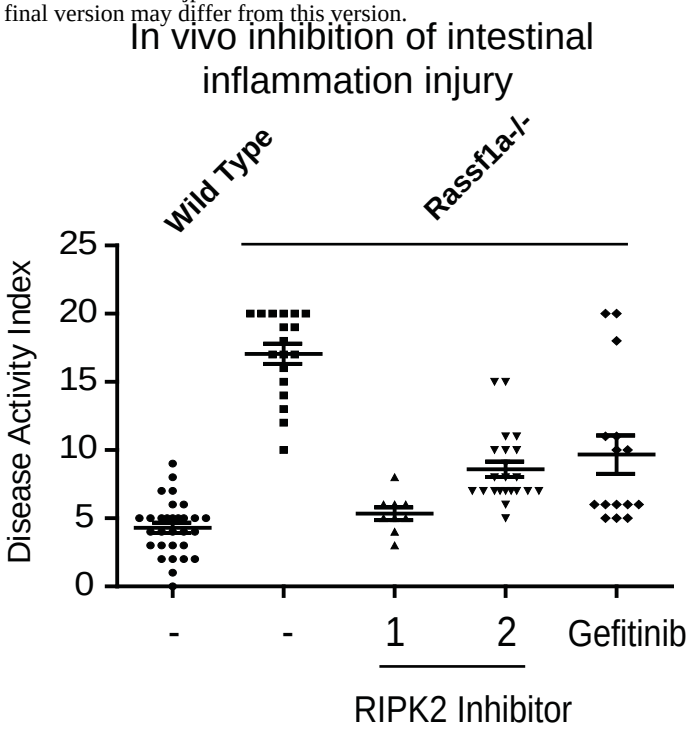

C

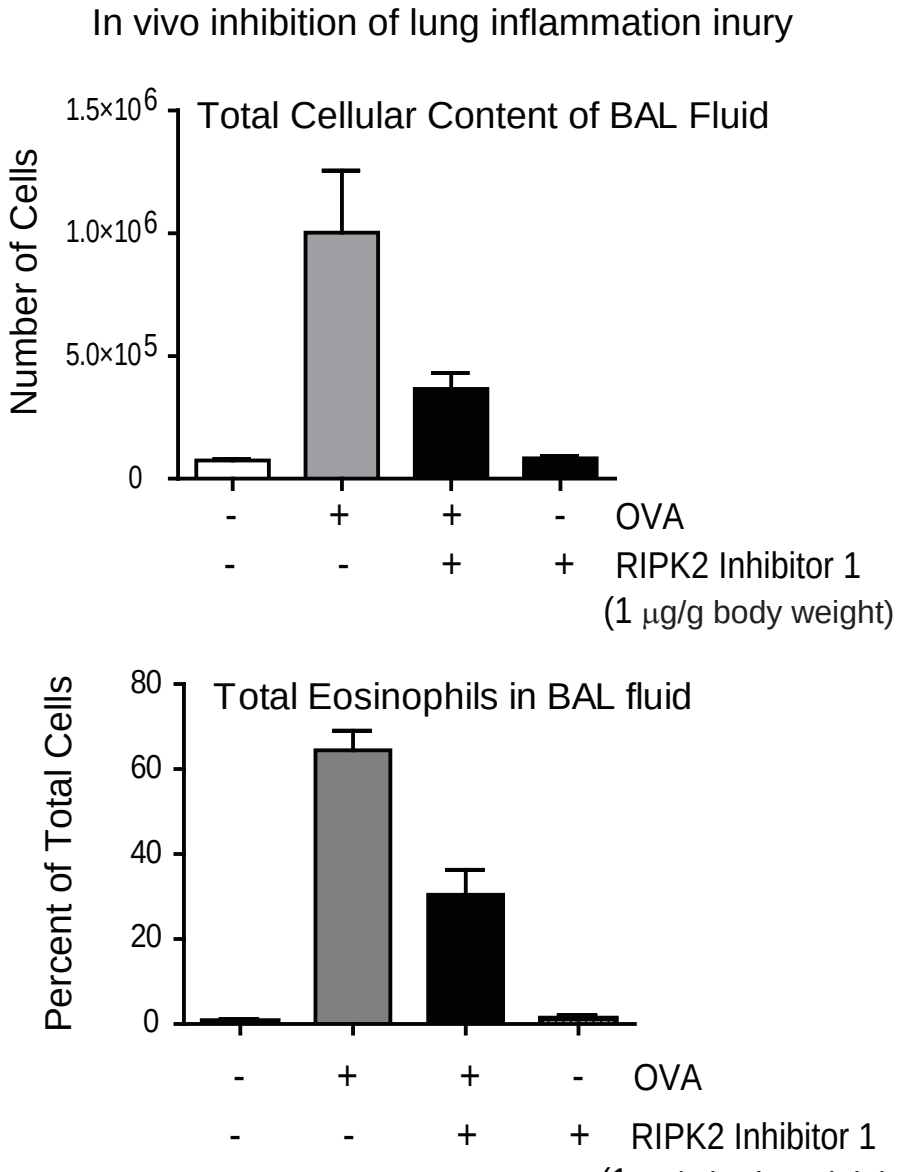

D

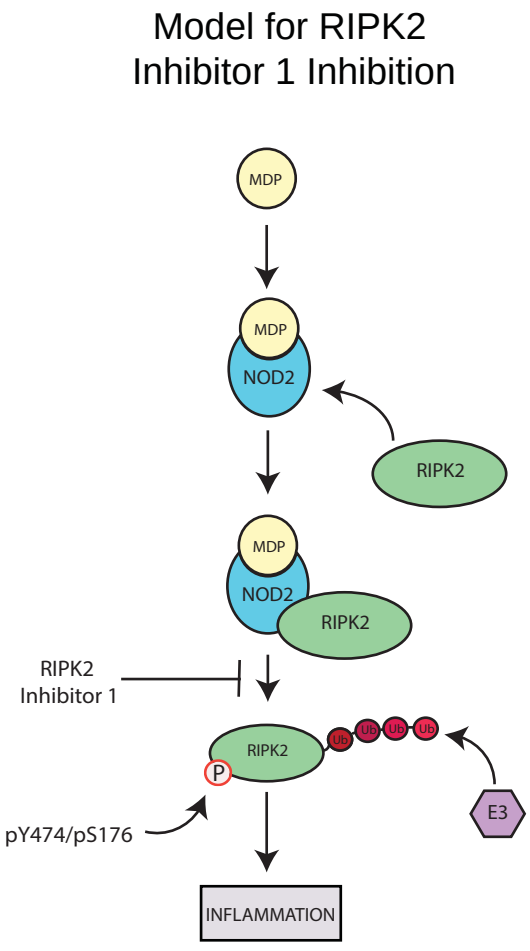

Salla et al, Figure 6